AMERICAN SOCIETY FOR MICROBIOLOGY | Journal of Virology®

VACCINES AND ANTIVIRAL AGENTS

Characterization of a Novel CD4 Mimetic Compound YIR-821 against HIV-1 Clinical Isolates

Kaho Matsumoto,[a,i] Takeo Kuwata,[a] William D. Tolbert,[b] Jonathan Richard,[c,d] Shilei Ding,[c,d] Jérémie Prévost,[c,d] Shokichi Takahama,[e] George P. Judicate,[a] Takamasa Ueno,[a] Hirotomo Nakata,[f] Takuya Kobayakawa,[g] Kohei Tsuji,[g] Hirokazu Tamamura,[g] Amos B. Smith III,[h] Marzena Pazgier,[b] Andrés Finzi,[c,d] Shuzo Matsushita[a]

[a]Joint Research Center for Human Retrovirus Infection, Kumamoto University, Kumamoto, Japan
[b]Infectious Disease Division, Department of Medicine, Uniformed Services University of the Health Sciences, Bethesda, Maryland, USA
[c]Centre de Recherche du CHUM (CRCHUM), Montreal, Quebec, Canada
[d]Département de Microbiologie, Infectiologie et Immunologie, Faculté de Médecine, Université de Montréal, Montreal, Quebec, Canada
[e]Laboratory of Immunosenescence, Center for Vaccine and Adjuvant Research, National Institutes of Biomedical Innovation, Health and Nutrition, Osaka, Japan
[f]Department of Hematology, Rheumatology, and Infectious Diseases, Graduate School of Medical Sciences, Faculty of Life Sciences, Kumamoto University, Kumamoto, Japan
[g]Institute of Biomaterials and Bioengineering, Tokyo Medical and Dental University, Tokyo, Japan
[h]Department of Chemistry, School of Arts and Sciences, University of Pennsylvania, Philadelphia, Pennsylvania, USA
[i]Graduate School of Medical Sciences, Kumamoto University, Kumamoto, Japan

ABSTRACT Small CD4-mimetic compound (CD4mc), which inhibits the interaction between gp120 with CD4, acts as an entry inhibitor and induces structural changes in the HIV-1 envelope glycoprotein trimer (Env) through its insertion within the Phe43 cavity of gp120. We recently developed YIR-821, a novel CD4mc, that has potent antiviral activity and lower toxicity than the prototype NBD-556. To assess the possibility of clinical application of YIR-821, we tested its antiviral activity using a panel of HIV-1 pseudoviruses from different subtypes. YIR-821 displayed entry inhibitor activity against 53.5% (21/40) of the pseudoviruses tested and enhanced neutralization mediated by coreceptor binding site (CoRBS) antibodies in 50% (16/32) of these. Furthermore, when we assessed the antiviral effects using a panel of pseudoviruses and autologous plasma IgG, enhancement of antibody-mediated neutralization activity was observed for 48% (15/31) of subtype B strains and 51% (28/55) of non-B strains. The direct antiviral activity of YIR-821 as an entry inhibitor was observed in 53% of both subtype B (27/51) and non-B subtype (40/75) pseudoviruses. Enhancement of antibody-dependent cellular cytotoxicity was also observed with YIR-821 for all six selected clinical isolates, as well as for the transmitted/founder (T/F) CH58 virus-infected cells. The sequence diversity in the CD4 binding site as well as other regions, such as the gp120 inner domain layers or gp41, may be involved in the multiple mechanisms related to the sensitive/resistant phenotype of the virus to YIR-821. Our findings may facilitate the clinical application of YIR-821.

IMPORTANCE Small CD4-mimetic compound (CD4mc) interacts with the Phe43 cavity and triggers conformational changes, enhancing antibody-mediated neutralization and antibody-dependent cellular cytotoxicity (ADCC). Here, we evaluated the effect of YIR-821, a novel CD4mc, against clinical isolates, including both subtype B and non-B subtype viruses. Our results confirm the desirable properties of YIR-821, which include entry inhibition, enhancement of IgG-neutralization, binding, and ADCC, in addition to low toxicity and long half-life in a rhesus macaque model, that might facilitate the clinical application of this novel CD4mc. Our observation of primary viruses that are resistant to YIR-821 suggests that further development of CD4mcs with different structural properties is required.

Editor Frank Kirchhoff, Ulm University Medical Center

Address correspondence to Shuzo Matsushita, shuzo@kumamoto-u.ac.jp.

The authors declare no conflict of interest.

[This article was published on 13 December 2022 with a reference missing and incorrect information in an author affiliation. These items were corrected in the current version, posted on 15 December 2022.]

Received 20 October 2022
Accepted 15 November 2022
Published 13 December 2022

KEYWORDS HIV-1, subtype B, non-B subtypes, clinical strain, monoclonal antibody, plasma IgG, CD4mc, envelope, conformation, mutation, entry inhibition, neutralization, ADCC, CD4mimic, envelope conformation, non-subtype B

Small CD4-mimetic compound (CD4mc) that inhibits the interaction of HIV-1 envelope (Env) gp120 with CD4, acts as an entry inhibitor and induces structural changes in the Env trimer through binding to the Phe43 cavity of gp120. CD4mc inhibits viral entry into host cells by competitive inhibition with CD4 and by premature allosteric activation of HIV-1 Env. Such premature activation leads to a series of conformational changes in Env, which irreversibly releases the energy necessary for viral fusion (1, 2). Furthermore, CD4mc can expose otherwise occluded epitopes on the native unliganded Env trimer that can be recognized by the host immune system, such as antibodies (Abs) targeting the coreceptor binding site (CoRBS) and the gp120 inner domain cluster A region (C1/C2 regions of Env) (3, 4). It is important to note that the HIV Env trimer is expressed on both the surface of viral particles and on HIV-1-infected cells (5). When cell surface Env is in an unliganded "closed" State 1 conformation, it cannot be recognized by most of the host Abs generated during natural infection (6). However, when Env is stabilized by CD4mc in the "open" conformation, CD4-induced (CD4i) epitopes become exposed and can be recognized by commonly elicited nonneutralizing CD4i Abs, thus sensitizing infected cells to antibody-dependent cellular cytotoxicity (ADCC) (7). This sensitization to ADCC requires sequential opening of the Env trimer. The successive binding of CD4mc, anti-CoRBS Abs, and anticluster A Abs results in the stabilization of an asymmetric Env conformation (State 2A) that is vulnerable to ADCC (4, 8). By stabilizing this "open" conformation, CD4mc can both neutralize the virus and stimulate ADCC, which has been proposed as a new strategy for HIV-1 eradication (4, 7–9).

CD4mc can potentially contribute to the control of HIV-1 replication and target the viral reservoir if it expresses Env. Upon treatment with CD4mc and CD4i Abs, a decrease in the viral reservoir and delayed viral rebound were observed in HIV-1-infected SRG-15 humanized mice after cessation of antiretroviral treatment (9). This study suggests that CD4mc-mediated sensitization of Env-expressing cells to ADCC-mediating Abs represents a promising therapeutic strategy for HIV-AIDS. However, in terms of the clinical applicability of CD4mc, it is essential to examine the effect on clinical isolates from the standpoint of diversity in the Env sequence.

We have developed a series of CD4mcs that have more optimal characteristics than the parental NBD-556 (10–15). After extensive structure-activity relationship analyses, we developed a CD4mc, YIR-821, that has improved anti-HIV activity and lower toxicity than NBD-556 (16) (Fig. 1). When conjugated with PEG units attached through an uncleavable linker, the novel CD4mc showed not only high anti-HIV activity with a low toxicity profile but also good pharmacokinetics in rhesus macaques (17). Additional data suggested that intramuscular injection of the PEG-conjugated compound was a more useful administration route than intravenous injection in maintaining a high blood concentration of the compound (17).

Like other CD4mcs, functional characterization of YIR-821 has been evaluated with a limited number of subtype B viruses. Because of the wide variety of Env sequences in primary isolates, it is important to examine the breadth of CD4mcs against clinical samples to determine their applicability in clinical settings. In this study, we assessed the functional properties of YIR-821 in terms of HIV-1 entry inhibition, neutralization, and binding enhancement by CoRBS Abs against a panel of viral envelopes from different subtypes. We also tested enhancement of ADCC against infected cells of two clinical isolates (CH58 and JR-FL). In further preclinical studies, we tested the effect of YIR-821 using a panel of pseudoviruses with envelopes from isolates from 31 subtype B HIV-1-infected Japanese individuals and 52 non-subtype B HIV-1-infected Tanzanian individuals. We observed entry inhibition activity, neutralization, and binding enhancement by YIR-821 in more than half of our clinical samples. Enhancement of ADCC was also observed in six selected subtype B clinical isolates. The results using this set of pseudoviruses and

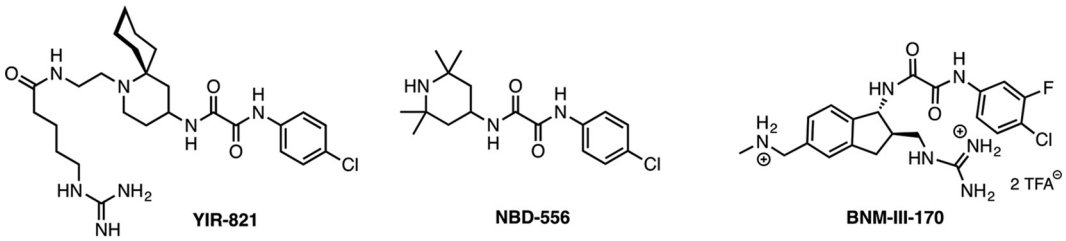

FIG 1 Chemical structure of YIR-821, NBD-556, and BNM-III-170.

autologous plasma IgG from each individual may facilitate the clinical application of YIR-821. The data may also be important for the selection of individuals that could benefit from the clinical application of CD4mcs.

RESULTS

Functional characterization of YIR-821. To evaluate the functional properties of YIR-821, we examined its ability to enhance the binding of a panel of mAbs against the Env V3 loop (KD-247 and 1C10), the CoRBS (916B2 and 4E9C), and the CD4 binding site CD4bs (VRC01), using PM1/CCR5 cells infected with BaL, JR-FL, or CH58T/F viruses in the presence or absence of YIR-821 (Fig. 2A). We observed a marked enhancement in the binding of V3 and CoRBS Abs for BaL. In the absence of YIR-821, binding of V3 mAbs was observed for both JR-FL and CH58T/F with a mild enhancement evident following the addition of the compound. In contrast, enhancement of CoRBS Ab binding was observed for all three viruses with YIR-821. This was consistent with the fact that the CoRBS is only accessible after engagement of Env trimer with CD4 or CD4mc. YIR-821 caused various degrees of conformational change that resulted in the enhancement of antibody binding to these three viruses.

We examined the direct antiviral effect of YIR-821 against pseudoviruses using the envelopes from strains BaL, JR-FL, and CH58 (Fig. 2B). Inhibition of viral entry was observed for BaL and CH58 viruses following YIR-821 binding to the target TZM-bl cells at low concentration, but it was not observed for JR-FL. We also evaluated the effect of YIR-821 on the enhancement of neutralization against strains BaL, JR-FL, and CH58 using the panel of mAbs described above. Neutralizing activity was assessed in the presence or absence of subinhibitory YIR-821 concentrations (20% of the maximal inhibitory concentration [IC_{20}]) for strains BaL and CH58. Given that JR-FL was the most resistant to YIR-821 ($IC_{50} > 50\ \mu M$), neutralization enhancement was examined in the presence of 20 μM YIR-821 (Fig. 2C). The enhancement of neutralization by YIR-821 was observed for anti-V3 and CoRBS Abs for strains BaL and CH58. However, with strain JR-FL, enhancement in neutralization was observed for CoRBS Abs only. As expected, no effect was observed for YIR-821 regarding the neutralization of the anti-CD4bs Ab VRC01 since YIR-821 and VRC01 compete for the same binding site.

Broad-spectrum entry inhibition and neutralization enhancement by YIR-821. We compared the entry inhibition activity of YIR-821 with that of the prototype CD4mc NBD-556 against panels of subtype B and C pseudoviruses (Fig. 3A). YIR-821 inhibited viral entry at a lower concentration in several samples compared with NBD-556. A significant difference in the mean IC_{50} values was evident between YIR-821 and NBD-556 when analyzed against the panel of subtype C pseudoviruses (Fig. 3B).

Next, we examined the effect of YIR-821 against a panel of HIV-1 pseudoviruses using the NIH standard subtype B, subtype C, and other subtypes (Fig. 3C). To evaluate the effect of YIR-821 on neutralization enhancement by CD4i Abs, we used two CoRBS Abs 4E9C and 916B2 (18, 19) in the presence or absence of YIR-821 at the concentration of the IC_{20} value for entry inhibition for the pseudoviruses that have an $IC_{20} < 20\ \mu M$. Neutralization enhancement was examined in the presence of 20 μM YIR-821 for the pseudoviruses that had an $IC_{20} > 20\ \mu M$ in the entry inhibition assay (see Table S1 in the supplemental material). The enhancement in neutralization in the presence

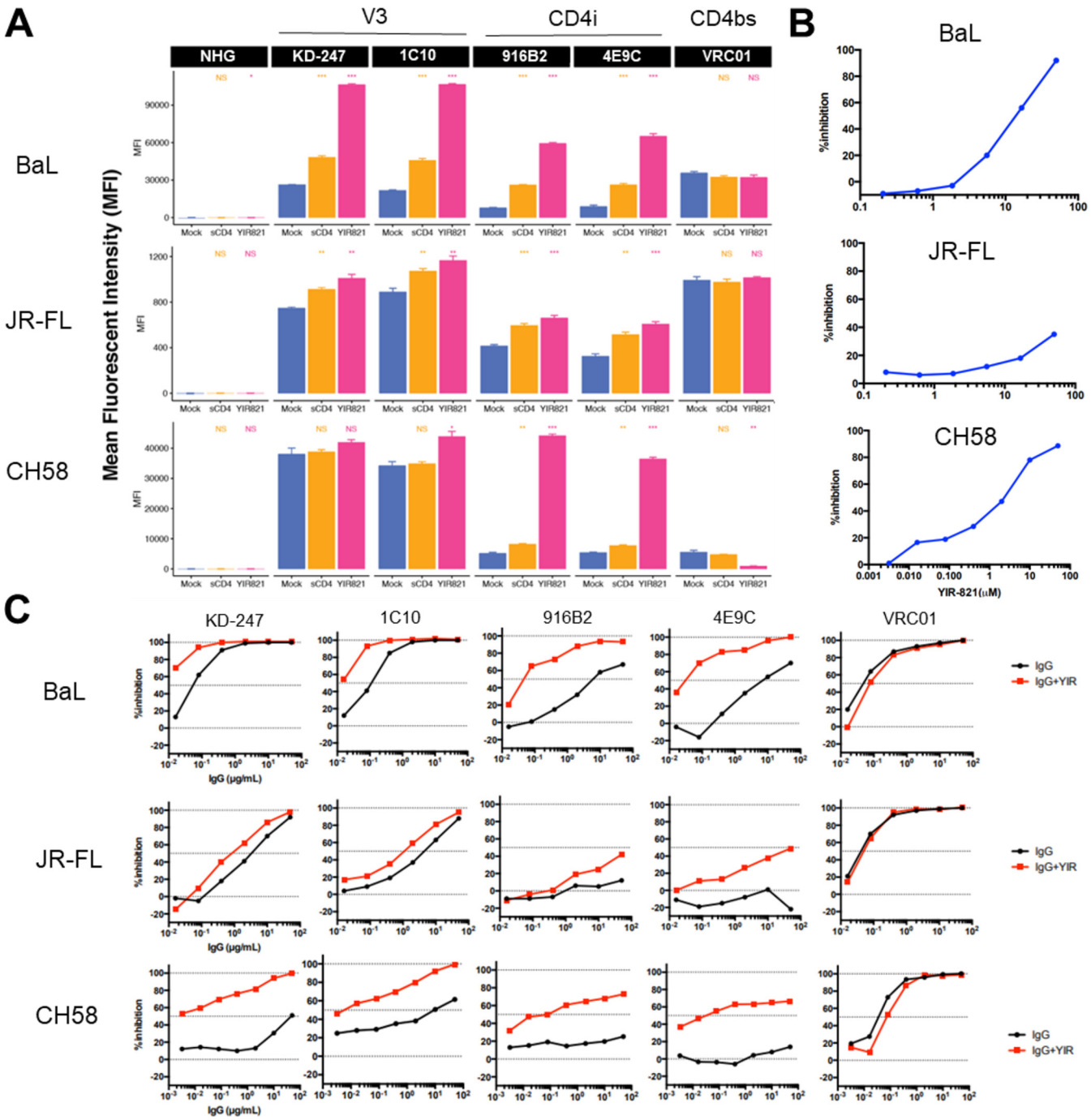

FIG 2 Functional characterization of YIR-821 (A) FACS analysis of the cell surface binding of a panel of mAbs against PM1/CCR5 cells infected with either BaL, JR-FL, or CH58 viruses in the presence or absence of YIR-821. Color code: blue, mock; yellow, sCD4; pink, YIR-821. Normal human IgG (NHG) was used as a negative control. Statistical significance was tested using an unpaired *t* test (*, $P < 0.05$; **, $P < 0.01$; ***, $P < 0.001$; ****, $P < 0.0001$; ns, nonsignificant). (B) The direct antiviral activity of YIR-821 was measured against BaL, JR-FL, and CH58 virions. (C) The enhancement of neutralization activity of a panel of mAbs by YIR-821 against BaL, JR-FL, or CH58 viral particles. Experiments were performed at least twice.

of YIR-821 was a >2-fold increase in neutralization for neutralization-sensitive pseudoviruses or the detection of neutralization at an IgG concentration <50 μg/mL for neutralization-resistant pseudoviruses.

Enhancement in neutralization by 4E9C in the presence of YIR-821 was observed in 6 out of 13 subtype B pseudoviruses (Fig. 3C), 6 out of 14 subtype C pseudoviruses, and 1 out of 5 pseudoviruses belonging to other subtypes. Enhancement of neutralization of 916B2 in the presence of YIR-821 was observed in 7 out of 13 pseudoviruses in

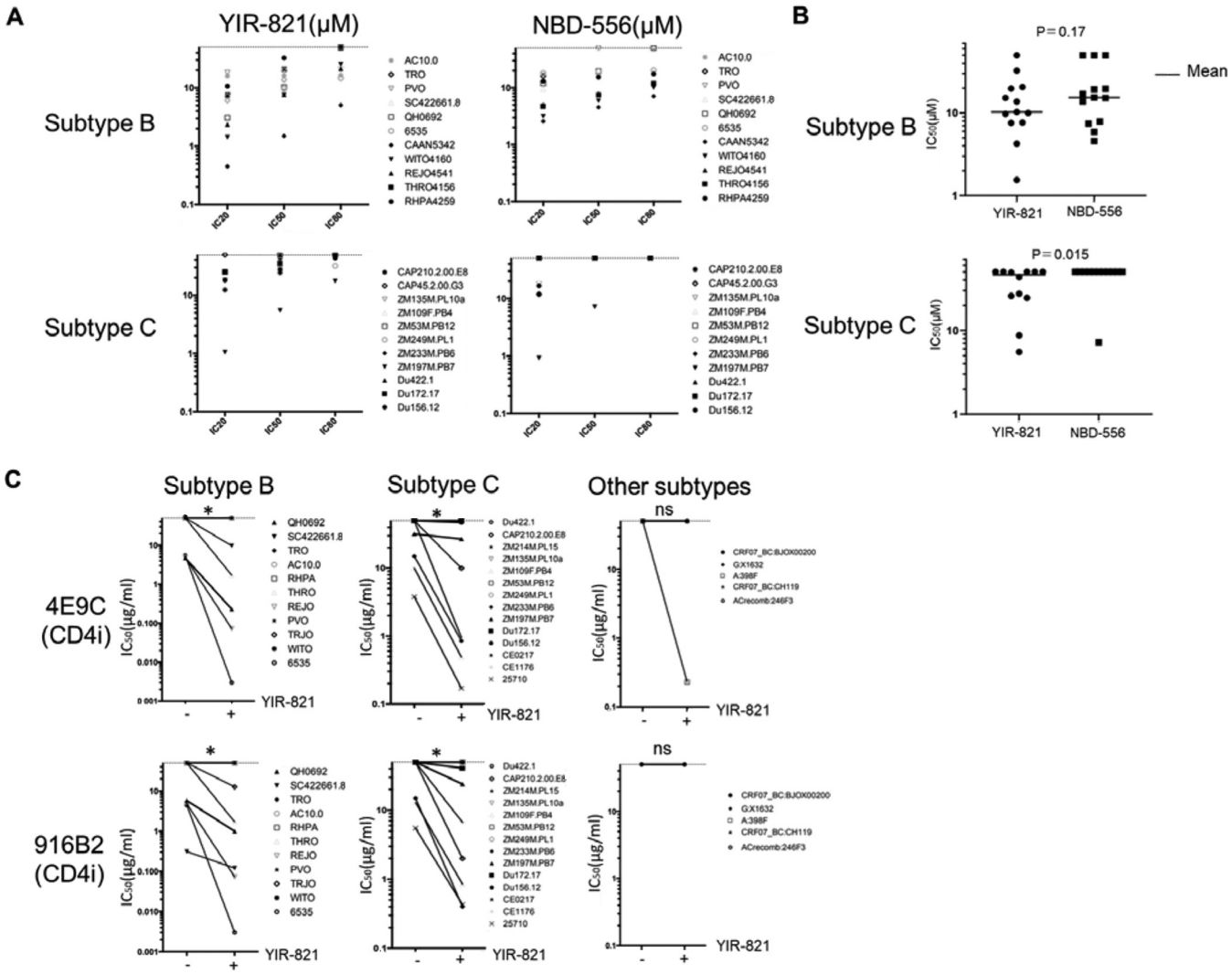

FIG 3 Comparison of the entry inhibition activity of YIR-821 with NBD-556 and broad-spectrum neutralization enhancement by YIR-821 against a panel of pseudoviruses of subtype B and C. (A) Entry inhibition activity of YIR-821 and NBD-556 against a panel of pseudoviruses of subtype B and C. The IC_{20}, IC_{50}, and IC_{80} values of YIR-821 (left) and NBD-556 (right) against each pseudovirus are shown. The dot bar is the maximum concentration used. Statistical significance was tested using a paired *t* test. (B) The IC_{50} values, including the mean for each CD4mc (line), are shown. (C) The reduction IC_{50} value, as a measure of 4E9C and 916B2 neutralization activity, by YIR-821 against a panel of pseudoviruses consisting of subtype B, subtype C, and other subtypes. TZM-bl cells were used as target cells. Statistical significance was tested using a paired *t* test (*, $P < 0.05$; **, $P < 0.01$; ***, $P < 0.001$; ****, $P < 0.0001$; ns, nonsignificant). Experiments were performed at least twice.

subtype B and 7 out of 14 pseudoviruses in subtype C. Overall, a marginal effect was observed for subtype C and the other subtypes. Taken together, these data suggest that YIR-821 can be effective in viral entry inhibition for 70% (14/20) of subtype B and 50% (7/14) of subtype C pseudoviruses. Neutralization enhancement for at least one of the CoRBS Abs was noted for 54% (7/13) of subtype B, 57% (8/14) of subtype C, and 20% (1/5) of the other pseudovirus subtypes (Table S1), suggesting that there is 50% (16/32) coverage of the pseudovirus panel for neutralization enhancement by YIR-821.

YIR-821 inhibits viral entry of HIV-1 enveloped pseudoviruses from subtype B and non-subtype B clinical isolates. To assess the clinical relevance of the above observations, we collected blood samples together with autologous and contemporaneous plasma IgG from 31 HIV-1-infected individuals to prepare a panel of pseudoviruses. These individuals were infected with subtype B virus and were treatment naive. We extracted viral genes and cloned the *env* genes from each of these samples, some of which have been reported previously (20–22). For non-B viruses, we collected blood

samples from 52 treatment-naive individuals (23). From these 52 samples, we obtained 55 clones of the *env* gene. In total, we cloned 16 subtype A, 13 subtype C, 7 subtype D, and 19 chimeric subtypes (4 of subtype AC, 6 of subtype AD, 1 of subtype ABC, 1 of subtype ACD, and 7 of subtype CD). We also obtained 43 autologous plasma IgG samples from these 52 individuals (12 from subtype A, 10 from subtype C, 5 from subtype D, and 16 from chimeric subtypes). Phylogenetic tree analysis of these 86 envelope gene sequences revealed diversity in each of the subtypes (Fig. 4A).

By cotransfection of each Env plasmid with a pSG3ΔEnv backbone, we generated pseudoviruses that were used to examine the entry inhibition activity of YIR-821 (Tables S2 and 3). We observed that 13 out of 31 of the pseudoviruses (42%) were inhibited by YIR-821 with an IC_{50} value of less than 50 μM, and 7 of these samples were highly sensitive to YIR-821 with an IC_{50} value of less than 5 μM in subtype B samples. In contrast, only 9 out of 16 subtype A pseudoviruses were inhibited by YIR-821 with an IC_{50} value of less than 50 μM with 6 out of these 9 pseudoviruses inhibited at an IC_{50} value of less than 5 μM. Of the subtype C pseudoviruses, 5 out of 13 were inhibited at an IC_{50} value of less than 50 μM YIR-821, with 3 of these 5 pseudoviruses inhibited at an IC_{50} value of less than 5 μM. Of the subtype D pseudoviruses, 6 out of 7 were inhibited at an IC_{50} value of less than 50 μM YIR-821, with 4 of these 6 pseudoviruses inhibited at an IC_{50} value of less than 5 μM. Of the chimeric subtype pseudoviruses, 13 out of 19 were inhibited at an IC_{50} value of less than 50 μM YIR-821, with 7 of these 13 pseudoviruses inhibited at an IC_{50} value less than 5 μM.

When we compared the IC_{50} values of YIR-821 in the entry inhibition assay between the different subtypes, including the 31 subtype B samples described in Fig. 4B, the pseudoviruses from subtype D were found to be the most sensitive to YIR-821, with 6 of the 7 viruses being scored as sensitive, as mentioned above (Table S3). Overall, the entry inhibition activity of YIR-821 against these clinical samples was 42% (13/31) for subtype B pseudoviruses and 60% (33/55) for non-B subtype pseudoviruses. When combined with the pseudovirus panel data, the total coverage of YIR-821 observed in the present study for subtype B pseudoviruses was 53% (27/51), with a comparable coverage of 53% (40/75) observed for non-B subtype pseudoviruses.

Enhancement of the neutralization and binding activity of plasma IgG and CoRBS Abs from patients by YIR-821 against pseudoviruses from clinical samples. We next examined the enhancement of neutralization by YIR-821 against 86 pseudoviruses with primary envelopes using plasma IgG obtained at the time of virus isolation and CoRBS Ab 4E9C (Fig. 5, Table S2 and 3). For the neutralization assay, we used YIR-821 at the IC_{20} dose determined for each pseudovirus in the entry inhibition assay and at 20 μM in the case of pseudoviruses with an $IC_{20} > 20$ μM. For subtype B pseudoviruses, we observed an enhancement in the IC_{50} value in the presence of YIR-821 for 15 out of 31 IgG samples for autologous plasma IgG neutralizing activity. In the case of 4E9C, a decreased IC_{50} value was observed for 16 out of the 31 samples in the presence of YIR-821. For subtype A pseudoviruses, YIR-821 enhanced neutralization activity in 10 out of 16 pseudoviruses for plasma IgG and 6 out of 16 pseudoviruses for 4E9C. In subtype C pseudoviruses, YIR-821 enhanced the neutralization activity in 5 out of 13 viruses for plasma IgG and 3 out of 13 pseudoviruses for 4E9C. For subtype D pseudoviruses, YIR-821 enhanced the neutralization activity in 3 out of 7 pseudoviruses for plasma IgG and 4 out of 7 pseudoviruses for 4E9C. For the chimeric subtype pseudoviruses, YIR-821 enhanced the neutralization activity in 10 out of 19 pseudoviruses for plasma IgG and 11 out of 19 pseudoviruses for 4E9C.

We observed a significant enhancement of autologous plasma IgG-mediated neutralization in the presence of YIR-821 in all five subtypes. For 4E9C-mediated neutralization, we observed significant enhancement in subtype B, subtype A, and the chimeric subtypes in the presence of YIR-821, while there was no significant change for the subtype C and subtype D pseudoviruses. Although subtype D was noted as being the most sensitive subtype in the entry inhibition assay, neutralization enhancement was not frequently detected in this subtype.

We also tested the enhancement of binding of plasma IgGs, 4E9C, and 17b in the presence of YIR-821 to the corresponding viral envelope. A significant enhancement in the

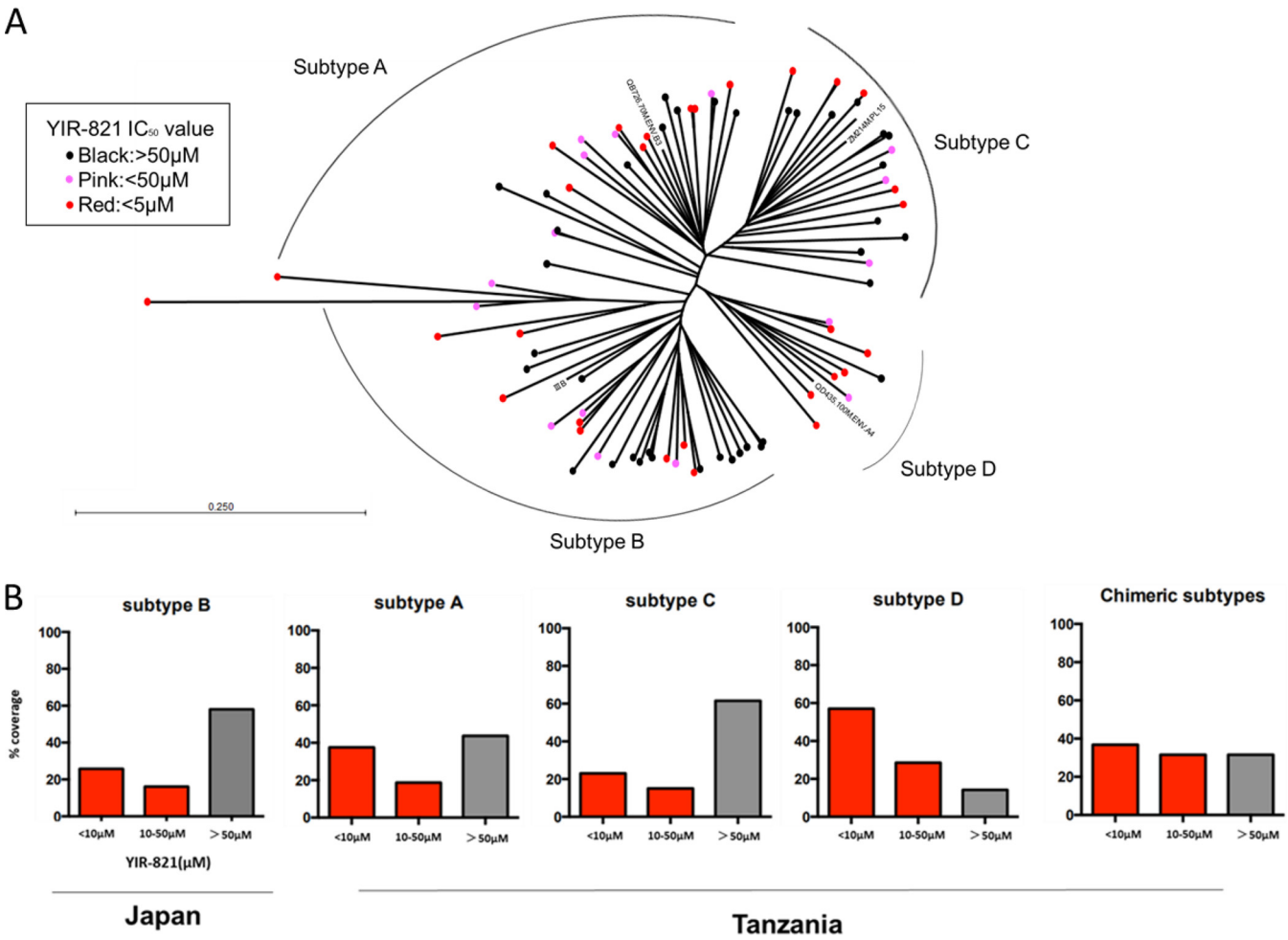

FIG 4 Phylogenetic tree of the envelope sequences of multiple subtypes of pseudovirus clinical isolates and the entry inhibition activity of YIR-821 against the same isolates. (A) Phylogenetic tree of the *env* genes from clinical isolates of subtypes A to D and chimeric subtypes. Reference sequences are included in the tree. Color code: black, >50 μM; pink, <50 μM and >5 μM; red, <5 μM for the YIR-821 IC_{50} value in the entry inhibition assay. (B) The direct antiviral activity of YIR-821 was measured against a panel of pseudoviruses using TZM-bl cells as the target cells. Experiments were performed at least twice. In these graphs, the bars representing samples that were sensitive to YIR-821 are colored in red (IC_{50} <50 μM), and the bars representing samples that were resistant to YIR-821 are colored in gray (IC_{50} >50 μM). Sample number: subtype B, 31; subtype A, 16; subtype C, 13; subtype D, 7; chimeric subtypes, 19.

binding of these Abs was observed in the presence of YIR-821 in all subtypes (Fig. 6). Particularly, a significant enhancement in binding was observed with almost all viral envelopes when CoRBS Abs were used to detect the conformational changes induced by YIR-821. For subtype A, enhancement in binding was not observed for plasma IgG in the presence of YIR-821, whereas significant enhancement in binding was observed for the two CoRBS Abs. The difference between plasma IgG, which consists of multiple anti-HIV Abs with different specificities, and CoRBS Abs, which have a single specificity, may account for the difference in enhancement seen for subtype A compared with the other subtypes.

Taken together, these data on the enhancement of IgG neutralization and binding activity suggest the broad activity of YIR-821 against various subtypes.

Evaluation of YIR-821 for the enhancement of anti-HIV antibody binding and ADCC against CH58- and JR-FL-infected CD4$^+$ T cells. To evaluate the enhancement of ADCC by YIR-821 using a combination of mAbs against the CoRBS (17b and 4E9C) and against the cluster A region (A32), we prepared CD4$^+$ T cells infected with CH58 as the target cells. First, we analyzed the binding of these mAbs in the presence of YIR-821 or another CD4mc, BNM-III-170 (Fig. 1), against the target cells (Fig. 7A). Enhancement in antibody binding was observed with a combination of two Abs (A32 with 17b or A32 with 4E9C), as detected by anti-human IgG or dimeric Fc receptor protein. This combination of

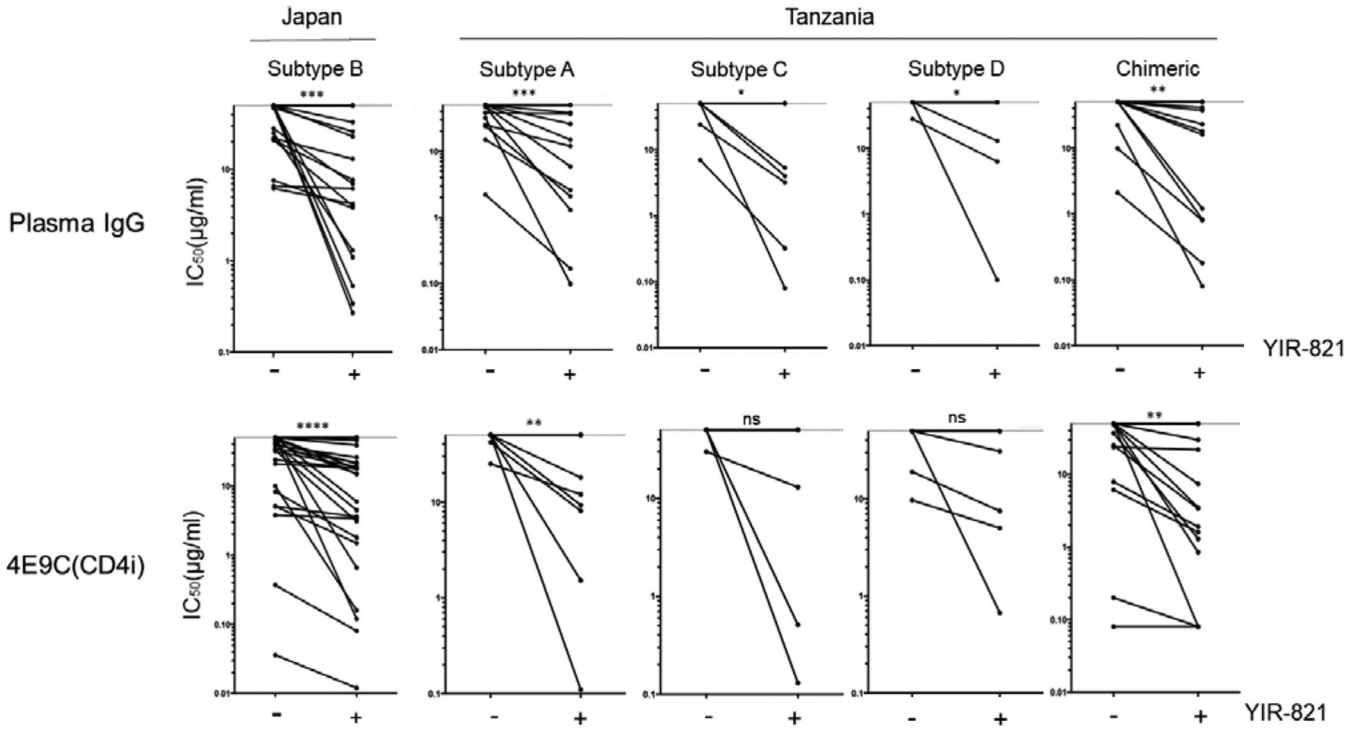

FIG 5 Enhancement of IgG neutralization activity by YIR-821 against pseudoviruses with envelopes from clinical isolates. The reduction of the IC_{50} value, as a measure of IgG neutralization activity by YIR-821 against pseudoviruses with envelopes from clinical isolates. The target cells were TZM-bl cells. Experiments were performed at least twice. Statistical significance was tested using a paired *t* test (*, $P < 0.05$; **, $P < 0.01$; ***, $P < 0.001$; ****, $P < 0.0001$; ns, nonsignificant).

two Abs resulted in increased interaction with soluble recombinant dimeric FcγRIIIa and increased ADCC against infected cells when using autologous primary human peripheral blood mononuclear cells (PBMCs) as effector cells (Fig. 7A). We also evaluated the enhancement of binding and ADCC using plasma samples from HIV-1-infected donors (Fig. 7B) against $CD4^+$ T cells infected with CH58 or JR-FL. Similar to what is shown in Fig. 7A, plasma binding enhancement together with greater FcγRIIIa binding and ADCC was observed in the presence of either CD4mc (YIR-821 or BNM-III-170), in the case of CH58-infected cells. In contrast, plasma binding enhancement, FcγRIIIa binding, and greater ADCC was only observed with BNM-III-170, not YIR-821, for JR-FL-infected target cells.

Enhancement of ADCC by YIR-821 against six selected subtype B viruses from clinical isolates. We examined the effect of YIR-821 on ADCC using autologous plasma IgG. For this purpose, we selected six samples that showed higher enhancement of 4E9C binding by YIR-821 from the 31 primary virus samples (Fig. 6), assuming that these viruses possess envelopes that are sensitive to the conformational changes induced by YIR-821. As shown in Fig. 8, ADCC against KB-01-08 was significantly enhanced in the presence of YIR-821 at an IgG concentration of 10 μg/mL. In the case of KB-02-03, KB-06-11, KB-16-09, and KB-17-07, enhancement in ADCC was observed in the presence of YIR-821 at IgG concentrations of 10, 1, and 0.1 μg/mL. Enhancement in ADCC by YIR-821 was observed for KB-20-17 at plasma IgG concentrations of 1 and 0.1 μg/mL. To characterize the conformational landscape of these primary envelopes, FACS analysis of the 293T cells transfected with the unmutated Env or the virus expressing the Env ectodomain (ecto-virus) were compared with the reactivity of a panel of conformational Abs in the presence or absence of YIR-821 (Fig. S1A–F). Enhancement in the binding of CoRBS Abs was observed for all cases, although the reactivity of CoRBS Abs in the absence of CD4mc suggested at least partially open conformations for the KB-06-11, KB-16-09, and KB-17-07 viruses.

Crystal structure of the Env gp120 subunit with YIR-821. To gain insight into the binding of YIR-821 to gp120, we determined the crystal structure of YIR-821 bound to clade CRF01_AE LM/HT 93TH057 gp120 extended core ($core_e$) (24). This gp120 contains

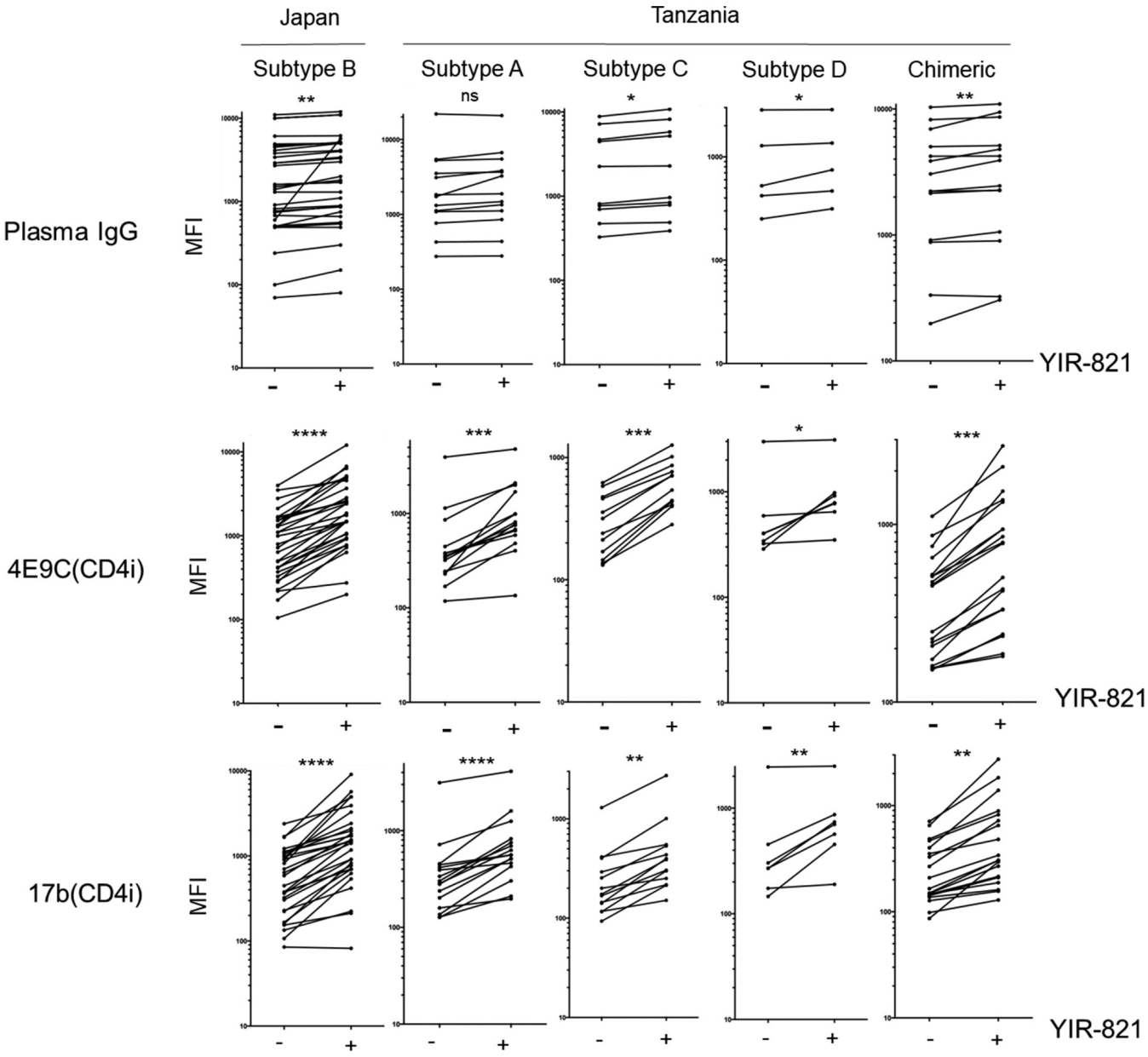

FIG 6 Enhancement of the IgG binding activities by YIR-821 against pseudoviruses with envelopes from clinical isolates. Binding assay involving flow cytometry with plasma IgG, 4E9C, and 17b. Transfected GFP-Env-expressing HEK293T cells were used. Experiments were performed at least twice. Statistical significance was tested using a paired *t* test (*, $P < 0.05$; **, $P < 0.01$; ***, $P < 0.001$; ****, $P < 0.0001$; ns, nonsignificant).

mutations within the mobile layers of gp120 to help stabilize the CD4-bound conformation, specifically His^{61} to Tyr, Gln^{105} to His, Val^{108} to Ile, Asn^{474} to Asp, Ile^{475} to Met, and Lys^{476} to Arg. It also has a Thr mutation at the base of the gp120 Phe43 cavity at position 375 to facilitate the binding of CD4mcs; clade A/E gp120s typically have His^{375} at this position, which prevents many CD4mcs from binding (24). To generate the complex, 200 nM YIR-821 was added to preformed crystals of LM/HT 93TH057 gp120 $core_e$ and the crystals were incubated for 4 h. The crystals were then frozen for data collection with the addition of 20% 2-methyl-2,4-pentanediol (MPD) as cryoprotectant. Data were collected on the Stanford Synchrotron Radiation Light Source (SSRL) beamline 12-2. Crystals were diffracted to 3.2 Å and the structure was solved by molecular replacement using PDB ID 6ONF as the starting model. Complete data collection and refinement statistics are presented in Table S4.

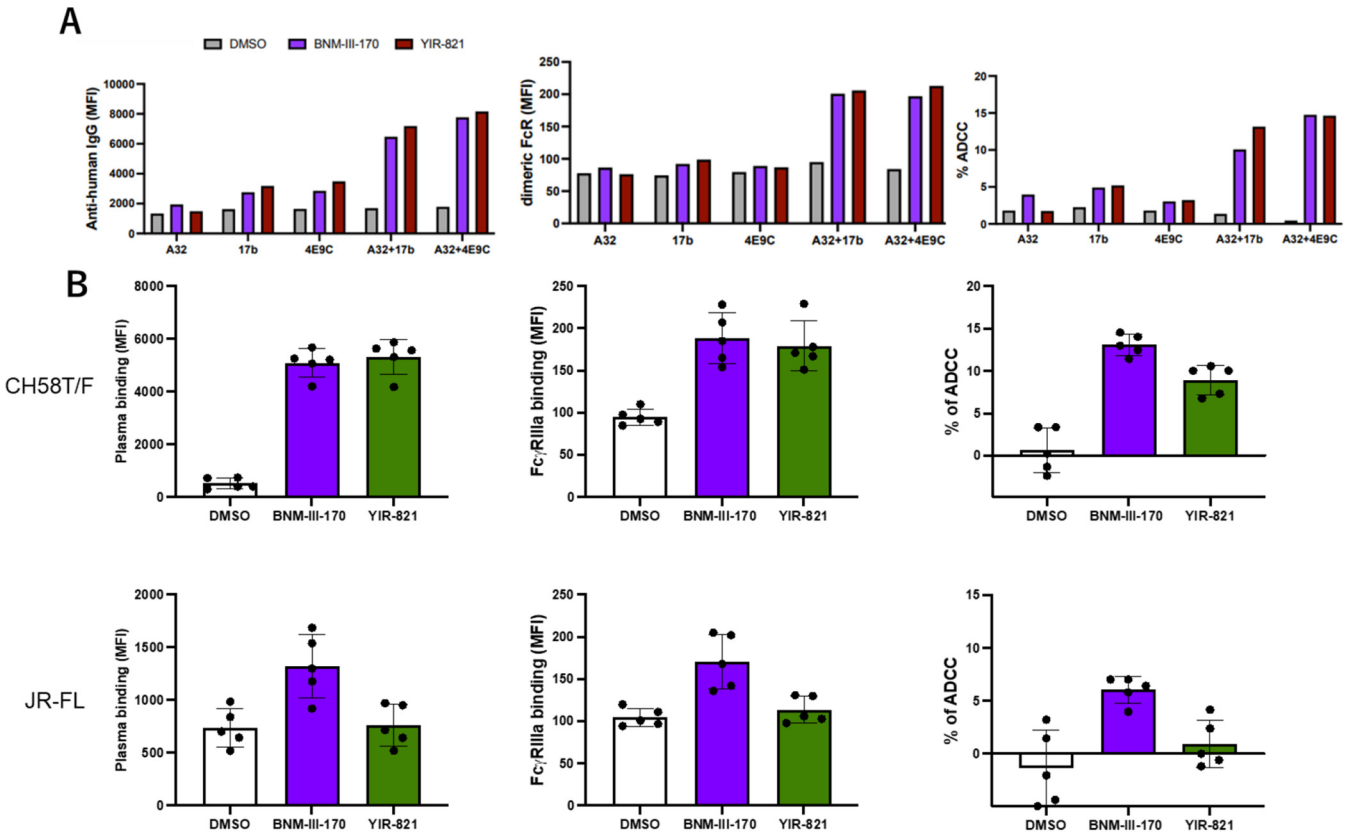

FIG 7 Enhancement of antibody binding and ADCC by CD4mcs. The enhancement of IgG binding was detected by anti-human IgG or dimeric FcγRIIIa protein, and ADCC was assessed using a FACS-based assay and CH58- or JR-FL-infected CD4$^+$ T cells in the presence of CD4mcs, YIR-821, or BNM-III-170. A panel of mAbs (A), as well as plasma samples from HIV-infected individuals (B), were tested. Experiments were performed at least twice.

Two alternate conformations of the compound were evident in the structure, one with the guanidino group interacting with residues in the same gp120 and one with the guanidino group interacting with residues of an adjacent gp120 in the crystal. The core *para*-chlorophenyl group, oxalamide linker, and azaspiro[5.5]undecane group were largely identical in the two conformations and formed the basis for the compound's interaction with the Phe43 cavity. In the first conformation, marked with a red arrow in Fig. 9, the guanidino group of the compound made contact with residues within the same gp120, while in the second conformation it made contact with residues in a neighboring gp120 in the crystal. Since the second conformation is only relevant within the crystallized complex, all subsequent analyses were conducted using the first conformation. YIR-821 buries a total of 774.7 Å^2, 477.3 Å^2 from the compound and 297.4 Å^2 from gp120. The *para*-chlorophenyl group and oxalamide linker insert themselves deeply into the Phe43 cavity sitting in a hydrophobic pocket formed by the aliphatic portions of the side chains of Thr^{375}, Glu^{370}, and Asn^{425}, the side chains of Phe^{382}, Trp^{112}, Val^{255}, Ile^{371}, Trp^{427}, and Met^{475}, and the main chain atoms of Thr^{257}, Phe^{376}, and Met^{426} (Fig. 9). Val^{255} in the figure sits underneath the *para*-chlorophenyl ring and is not visible in the orientation shown. The azaspiro[5.5]undecane group sits at the top of the cavity and only interacts with Met^{475}, Trp^{427}, and the aliphatic portion of the Asp^{474} side chain. The guanidino group extends the reach of YIR-821 to contact residues outside the cavity, primarily Asp^{477} and Thr^{283}.

The mode of binding for YIR-821 is like that of its parent compound NBD-556 (25) and another derivative compound of NBD-556, BNM-III-170 (24, 26) (Fig. 1). NBD-556 buries a total surface area of 649.2 Å^2, 433.0 Å^2 from the compound and 216.2 Å^2 from gp120, which is 125 Å^2 less than YIR-821. The buried surface area of YIR-821 is more comparable to that of BNM-III-170, which buries 796.4 Å^2, 485.2 Å^2 from the compound

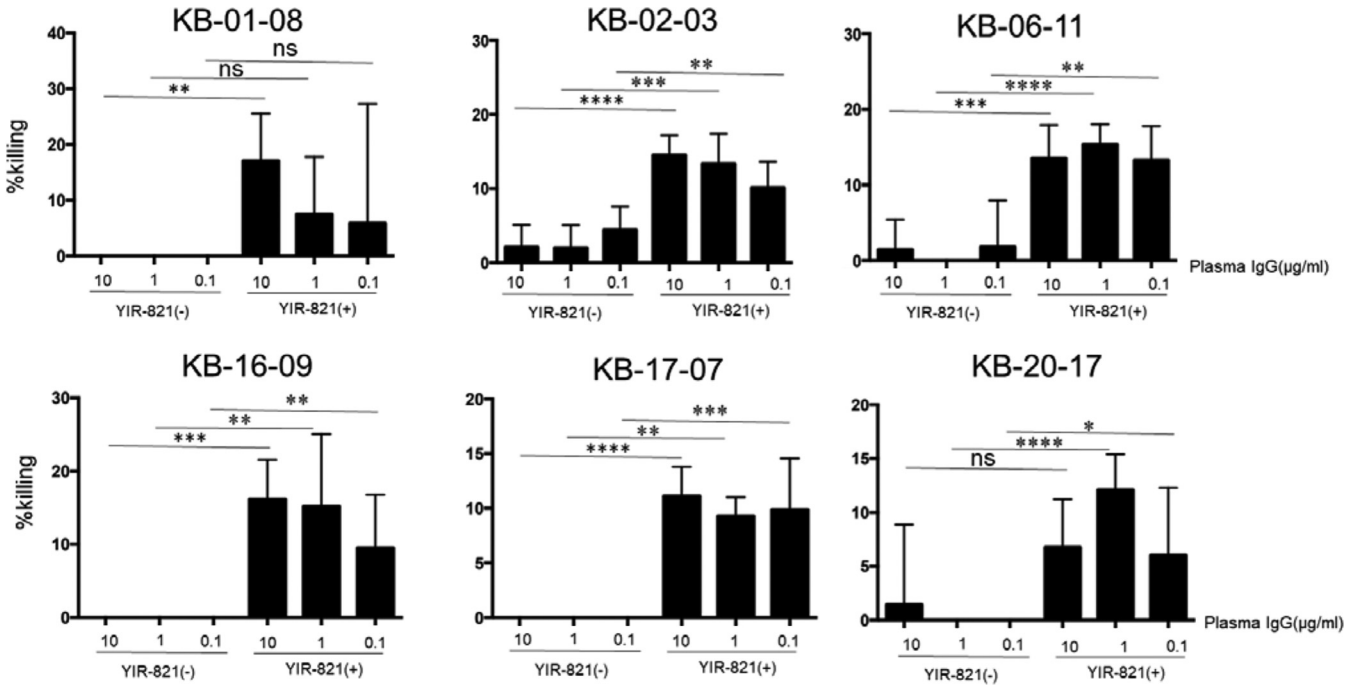

FIG 8 Enhancement of ADCC by YIR-821 against six selected subtype B viruses from clinical isolates. CEM.NKR-CCR5 cells infected with viruses with Env ectodomain from six individuals were used as target cells. The effector cells were N6 cells. The concentration of serum IgG was 10, 1.0, or 0.1 μg/mL. YIR-821 was used at 20 μM. NHG was used as a negative control and <3% killing was detected in this control in all experiments. Statistical significance was tested using an unpaired *t* test (*, $P < 0.05$; **, $P < 0.01$; ***, $P < 0.001$; ****, $P < 0.0001$; ns, nonsignificant).

and 311.2 Å^2 from gp120. YIR-821 and NBD-556 share the core *para*-chlorophenyl group, while BNM-III-170 adds a fluorine to the *para*-chorophenyl ring. All three compounds have an oxalamide linker with different head groups. The oxalamide linker nitrogens in both NBD-556 and BNM-III-170 make hydrogen bonds to the carbonyl oxygens of Asn^{425} and Gly^{473}, which is similar to the conformation seen for the oxalamide linker in YIR-821. The head group for all three compounds sits at that top of the Phe43 cavity. While NBD-556 uses its head group to interact primarily with the aliphatic part of the Asp^{474} side chain, YIR-821 and BNM-III-170 use their head groups to reach residues outside the Phe43 cavity. BNM-III-170 increases the interaction with Asp^{474} relative to NBD-556 and adds nitrogen-mediated hydrogen bonds to the carbonyl oxygens of Met^{426} and Gly^{472}. YIR-821 also interacts strongly with Asp^{474} but has additional contacts to Asp^{477} and Thr^{283}.

To examine the correlation between the effect of YIR-821 and the envelope sequence, we analyzed mutations in contact residues that scored more than 10 Å^2 with the buried surface area (BSA) (Fig. 9) together with residues in the CD4 binding cavity, including Asp^{368} (CD4bs), and layers 1, 2, and 3 (24) in each sequence (Tables S2 and 3). When we focused on the effect of entry inhibition activity by YIR-821 in subtype B viruses, we found that all six cases with the Ser^{375} to Thr mutation were sensitive to entry inhibition by YIR-821 (i.e., with an IC_{50} value for YIR-821 of less than 50 μM). In contrast, in non-B subtype viruses, specifically in the chimeric CD viruses, all four cases with the Ser^{375} to Thr mutation were sensitive to entry inhibition by YIR-821. The Ser^{375} to Thr mutation in the other subtypes was rare among our samples. Of note, one strain from subtype A1 (ID 83.1), with a cavity-filling M375 residue, was found to be mainly resistant to YIR-821 antiviral activity.

It may be interesting to note that four out of six samples with the Ser^{375} to Thr mutation in subtype B also had a His^{105} to Gln mutation in layer 2. Sample ID 25.2 of subtype A1 with the Ser^{375} to Thr mutation was found to be sensitive to YIR-821, while sample ID 25.6, which was obtained from the same donor, was not sensitive to CD4mc, further suggesting the importance of the Ser^{375} to Thr mutation for sensitivity to entry inhibition by YIR-821. No other mutations were found at YIR-821 contact residues

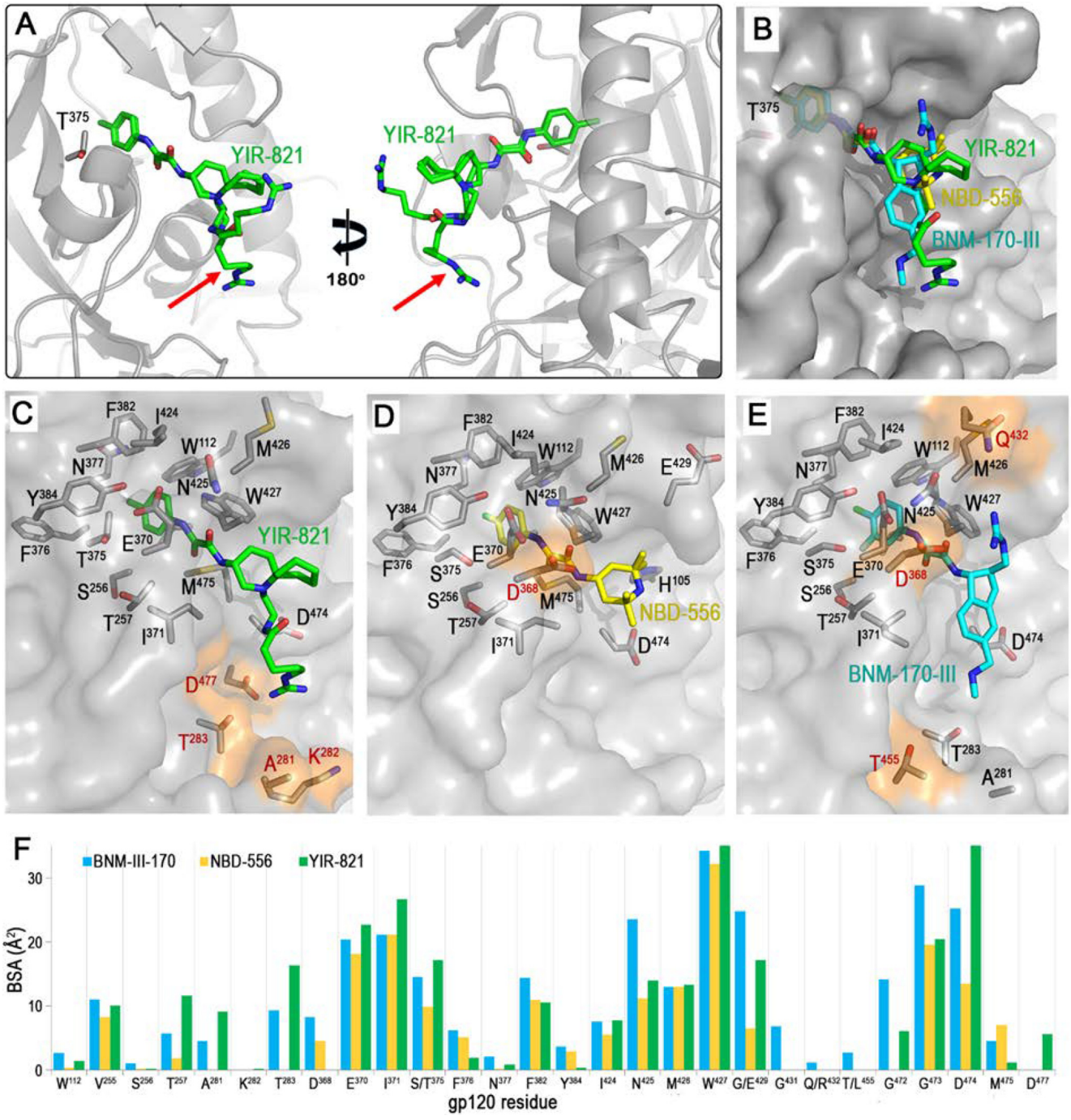

FIG 9 Detailed structural information on YIR-821 bound to the clade A/E LM/HT 93TH057 gp120 $core_e$. (A) 180° views of YIR-821 within the Phe43 cavity of HIV-1 gp120. YIR-821 displays two alternate conformations in the crystal. The first conformation, marked with a red arrow, only contacts gp120 residues in the same asymmetric unit, while the second conformation also contacts gp120 residues of an adjacent asymmetric unit. Panels B, C, and F only describe the details of the first conformation marked with a red arrow in panel A. (B) Comparison of YIR-821 binding to gp120 (shown in green), to parental compound NBD-556 (PDB ID 3TGS) (shown in yellow), and to BNM-III-170 (PDB ID 6UT1) (shown in cyan). Structures were aligned based on alpha carbon positions and gp120 is shown as a gray surface. Carbon atoms are colored as indicated, nitrogen atoms are blue, oxygen atoms are red, chlorine atoms are green, and fluorine atoms are light gray. (C) The details of YIR-821 binding to gp120. YIR-821 is colored as in panel B with gp120 shown as a gray surface. The gp120 residues contributing to compound binding are shown as sticks. Residues that are unique to YIR-821, compared with NBD-556 or BNM-III-170, are highlighted in orange and labeled in red. (D) The details of parental NBD-556 binding to gp120. NBD-556 is colored as in panel B with gp120 residues contributing to binding shown as sticks. Residues that are unique to NBD-556, compared with YIR-821, are highlighted in orange and labeled in red. (E) The details of BNM-III-170 binding to gp120, colored as in panel B with gp120 residues contributing to binding shown as sticks. Residues that are unique to BNM-III-170, compared with YIR-821, are highlighted in orange and labeled in red. (F) Bar chart of the buried surface area for each gp120 residue for the three structures, colored as indicated. For clarity, only those residues contributing to binding are shown.

Val^{255}, Thr^{257}, Glu^{370}, Phe^{382}, Asn^{425}, Trp^{427}, Gly^{473}, or Met^{475} in layer 3 or Asp^{368} in the CD4 binding site of the 31 subtype B samples tested (Table S2). Among the 52 non-B subtype samples, the Thr^{257}, Glu^{370}, Phe^{382}, Trp^{427}, Gly^{473}, and Asp^{368} contact residues showed no mutations relative to the Env consensus sequence (Table S3). No clear correlation was found between these mutations and the binding and/or neutralization enhancement of YIR-821 (Fig. S2). A significant *P* value was obtained, as seen in the lower left panel of Fig. S2, but this represented an inverse correlation. It is possible that the susceptibility to YIR-821 is more often dependent upon a combination of mutations outside the Phe43 cavity rather than a single point mutation within the cavity.

DISCUSSION

CD4mc possess three valuable complementary antiviral properties: entry inhibition by direct inactivation of viral particles, sensitization of viral particles to neutralization by otherwise nonneutralizing Abs, and sensitization of HIV-1-infected cells to ADCC-mediated killing (27). Recent advances in the development of a series of CD4mcs that engage Env in a CD4-like manner and that induce similar conformational changes resulted in the exposure of CD4i epitopes, which enabled us to test these antiviral activities.

In this study, we observed the antiviral properties of YIR-821 not only for subtype B but also for non-subtype B primary isolates. Although there were some differences in the effects among the subtypes, it is important to note that there were fully susceptible and resistant viruses in each subtype (Fig. 4B). Prévost et al. (24) previously reported that a point mutation at position 375 in Env affects the binding affinity of CD4mc, because this residue sits at the base of the Phe43 cavity of the CD4 binding site and directly influences the binding of CD4mc. CH58 virus with threonine at position 375 was found to be highly susceptible to the CD4mc, BNM-III-170 (24).

We estimated that the three functions of CD4mc (i.e., entry inhibition, enhancement in neutralization, and sensitization of HIV-1-infected cells to ADCC-mediated killing) are often but not always closely related. For example, most subtype D pseudoviruses were sensitive to the entry inhibition activity of YIR-821, but we observed only a few cases with enhancement in neutralization. This observation may suggest that the ability of CD4mcs to inhibit viral entry in subtype D viruses is linked to their capacity to induce gp120 shedding, which results in the inactivation of the virus, as previously reported by Selhorst et al. (28) and Anang et al. (29). Antiviral activity may therefore not necessarily require conformational changes in the Env trimer (29). The enhancement of CoRBS Ab binding was observed in many cases in FACS analyses, but the enhancement of neutralization was limited to approximately 50% of cases. This suggests that additional factors are required for neutralization by CoRBS Abs in the presence of YIR-821. Two mechanisms are thought to be involved in this HIV-1 resistant/sensitive phenotype to CD4mcs, as recently described by Anang et al. (29). One mechanism is sequence diversity of the CD4-binding domain of gp120. Although direct binding of CD4mcs was not examined, binding affinity to gp120 may depend on amino acid usage in the CD4-binding site of gp120, including sites within the contact region of YIR-821, such as 375T/S. The binding affinity of the cell-associated CD4 molecule to gp120 may be significantly higher than that of CD4mcs, as was described for soluble CD4 (sCD4). Daar et al. (30) previously reported that some viruses that still use CD4 as a receptor have resistance to sCD4 via this mechanism. Taking this into consideration, it is possible that viruses that are resistant to YIR-821 in an entry inhibition assay have a susceptible phenotype to a conformational change that allows neutralization/ADCC enhancement. The second mechanism of resistance is based on the susceptibility of individual Env proteins to induce transitions from State 1 to downstream conformations in the presence of CD4mcs. Viruses with Env proteins that have more stable State 1 conformations and are therefore less prone to transition from State 1 have been shown to exhibit greater resistance to CD4mcs. Sequence diversity in the CD4 binding site, as well as other regions, such as the gp120 inner domain layers or gp41, might be involved in this phenotype (24, 30, 31).

Finally, strong ADCC was detected for all six of the test samples in the presence of

YIR-821. Plasma IgG contains a variety of ADCC-mediating Abs in addition to those binding to the CoRBS such as those targeting the gp120 inner domain cluster A region, which are nonneutralizing. This might explain why sensitization of HIV-1-infected cells to ADCC-mediated killing by YIR-821 can be observed more readily than neutralization by CD4-induced (CD4i) antibodies. In summary, our work demonstrates that YIR-821 has many of the desirable properties that might facilitate the clinical application of a CD4mc.

MATERIALS AND METHODS

Ethics statement. Human blood samples were collected after signed informed consent was obtained in accordance with the study protocol approved by the Ethics Committee for Clinical Research and Advanced Medical Technology at the Kumamoto University School (approval no. 1637).

Written informed consent was obtained from all study participants in the Montreal Primary HIV Infection Cohort (32, 33) and the Canadian Cohort of HIV Infected Slow Progressors (34–36), and research adhered to the ethical guidelines of CRCHUM and was reviewed and approved by the CRCHUM institutional review board (ethics committee approval no. CE 16.164 - CA). Research adhered to the standards indicated by the Declaration of Helsinki. All participants were adults who provided informed written consent prior to enrollment in accordance with Institutional Review Board approval.

Cells and reagents. HEK293T and TZM-bl cells were provided by the NIH AIDS Reagent Program, Division of AIDS, NIAID, USA. CEM-NKR-CCR5-Luc cells with LTR-Luc, N6 cells, and the NK cell line KHYG-1 were provided by David T. Evans (37). HEK293T and TZM-bl cells were maintained in Dulbecco's modified Eagle's medium (DMEM; Nacalai Tesque, Inc., Kyoto, Japan) supplemented with 10% heat-inactivated fetal bovine serum (FBS; Mediatech Inc., Corning, Manassas, VA, USA). CEM.NKR-CCR5 cells with LTR-Luc were maintained in RPMI 1640 (Fujiflm, Osaka, Japan) supplemented with 10% FBS, 2 mM Glutamax, and 0.1 mg/mL Primocin (R10). N6 cells and the human NK cell line KHYG-1 expressing human CD16 were maintained in R10 medium supplemented with 1 μg/mL Cs-A and 5 U/mL IL-2. PM1/CCR5 cells (41) were maintained in RPMI 1640 medium containing 10% FBS. The generation of CD4mc YIR-821 was previously reported (38). PBMCs and $CD4^+$ T cells were isolated, activated, and cultured as previously described (39). Briefly, PBMCs were obtained by leukapheresis from HIV-negative individuals and $CD4^+$ T lymphocytes were purified from resting PBMCs by negative selection using immunomagnetic beads, according to the manufacturer's instructions (StemCell Technologies, Vancouver, BC, Canada), and were activated with phytohemagglutinin-L (10 μg/mL) for 48 h and then maintained in RPMI 1640 complete medium supplemented with recombinant interleukin-2 (rIL-2) (100 U/mL).

Viral production and infection. Vesicular stomatitis virus G (VSVG) pseudoviruses were produced and titrated as previously described (24). Viruses were used to infect activated primary $CD4^+$ T cells from healthy HIV-1-negative donors by spin infection at 800 $\times$ *g* for 1 h in 96-well plates at 25°C.

Plasma IgG and monoclonal antibodies. In total, 31 plasma IgGs from subtype B HIV-1-infected individuals and 46 plasma IgGs from non-subtype B HIV-1-infected individuals were purified using HiTrap rProtein A FF columns (GE Healthcare, USA) or by a spin column-based antibody purification kit (COSMO BIO, APK-10A). 1C10 (19), KD247 (19), 916B2 (19, 20), 4E9C (19, 20), 17b (39), and A32 (40) have been previously reported.

Cloning of full-length *env* genes from HIV-1-infected individuals. Env cloning of subtype B virus was performed as previously described (20–22). Briefly, viral mRNA from the plasma of each individual was extracted using an QIAmp viral RNA kit (Qiagen, cat. no. 52904). Reverse transcription was performed using SuperScript III reverse transcriptase (Invitrogen, cat. no. 12574026) with primer Env-N (5′-CTG CCA ATC AGG GAA TGA GCC TTG TGT-3′). Then, nested PCR was performed using the Tks Gflex DNA polymerase kit (TaKaRa, cat. no. R060A) with primers, *env*-OF (5′-TAG AGC CCT GGA AGC ATC CAG GAA G-3′) and *env*-OR (5′-TTG CTA CTT GTG ATT GCT CCA TGT-3′) for the first PCR, and BIF-F (5′-CTT GGT ACC GAG CTC GTT AGG CAT CTC CTA TGG CAG GAA GAA G-3′) and BIF-R (5′-GGG AGG GAG AGG GGC GGT CTC GAG ATA CTG CTC CCA CCC-3′) for the second PCR. The second PCR product was extracted from a 1% agarose gel using the QIAquick gel extraction kit (Qiagen, cat. no. 28704). The resulting fragment was transformed into the BamHI–HF restriction site of the pcDNA3.1-IRES-EGFP vector (New England BioLabs, cat. no. R3136S) using the Gibson assembly master mix (New England BioLabs, cat. no. E2611S).

Production of pseudovirus for entry inhibition assay and neutralization assay. Each Env plasmid was cotransfected with the pSG3ΔEnv backbone into HEK293T cells. After 48 h of transfection, the supernatant was stored at −80°C. The median tissue culture infectious dose ($TCID_{50}$) of each pseudovirus was determined using TZM-bl cells.

Entry inhibition assay using pseudovirus. Serially diluted YIR-821 and pseudovirus (400 $TCID_{50}$) were incubated for 1 h, and 100 μL of TZM-bl cells (1 $\times$ 10^5 cells/mL) were added. After incubation for 48 h, the galactosidase activity was measured using a galactosidase substrate (Tropix Gal-Screen substrate, Applied Biosystems) and an EnSpire multimode plate reader (PerkinElmer, MA, USA). The relative light units (RLU) were compared to calculate the reduction in infectivity and 50% of the maximal inhibitory concentration (IC_{50}) was calculated using nonlinear regression.

Antibody neutralization assay using pseudovirus. The neutralization activity of Abs was determined as previously described (42). In brief, serially diluted antibody and pseudovirus (400 $TCID_{50}$) were incubated for 1 h with or without YIR-821, and 100 μL of TZM-bl cells (1 $\times$ 10^5 cells/mL) were added. After incubation for 48 h, the galactosidase activity was measured using galactosidase substrate (Tropix Gal-Screen substrate,

Applied Biosystems) and an EnSpire multimode plate reader (PerkinElmer). The IC_{20} of YIR-821 was used in the entry inhibition assay, and 20 μM was set as the cutoff value. The RLUs were compared to calculate the reduction in infectivity and the IC_{50} was calculated using nonlinear regression.

IgG binding assay by flow cytometry. The detection of IgG bound to Env-expressing HEK293T cells was carried out as previously described (43). Briefly, 293T cells were transfected with a plasmid expressing both HIV-1 Env and enhanced green fluorescent protein (EGFP). After 48 h of transfection, the cells were incubated with or without YIR-821 (20 μM) for 15 min at room temperature (RT), then stained with primary antibody (2 μg/mL) for 15 min at RT. The cells were washed twice with PBS containing 0.2% BSA and incubated with allophycocyanin (APC)-conjugated AffniPure F(ab')2 fragment goat antihuman IgG (H+L) (Jackson Immuno Research, West Grove, PA, USA) for 15 min at RT. Cells were fixed with PBS containing 10% formalin and analyzed using the FACS Canto II (BD Biosciences, San Jose, CA, USA). The reactivity of the Abs was analyzed after gating the EGFP+ cells using FlowJo v10.5.3 (Tree Star, San Carlos, CA, USA). All experiments were performed at least twice independently, and representative results are shown.

Generation of infectious molecular clones for the ADCC assay using infected CEM.NKr-CCR5 cells and N6 cells. The vector pNL4.3 env.ecto was generated as previously reported (43, 44). Briefly, replication-competent infectious molecular clones were designed to include six selected *env* genes in pNL4-3 (GenBank accession number AF324493). The region of the *env* gene that encodes the ectodomain was amplified by primers. The amplified fragment was replaced with the corresponding region of pNL4-3 using the GeneArt seamless cloning and assembly enzyme mix (Invitrogen, Carlsbad, CA, USA), generating plasmid containing the *env* ectodomain from each individual.

Cell surface staining of infected cells. Cell surface staining of primary infected cells was performed at 48 h postinfection. Mock-infected or HIV-1-infected primary $CD4^+$ T cells were incubated for 30 min at 37°C with anti-Env monoclonal Abs (mAbs) (5 μg/mL) or plasma (1:1,000 dilution). Cells were then washed once with PBS and stained with the appropriate Alexa Fluor 647-conjugated secondary antibody (2 μg/mL) for 20 min at RT. After one more PBS wash, cells were fixed in a 2% PBS-formaldehyde solution. Alternatively, the binding of anti-Env Abs was detected using a biotin-tagged dimeric recombinant soluble FcγRIIIa (0.2 μg/mL) followed by the addition of Alexa Fluor 647-conjugated streptavidin (Thermo Fisher Scientific; 2 μg/mL). Infected cells were then permeabilized using the Cytofix/Cytoperm fixation/permeabilization kit (BD Biosciences, Mississauga, ON, Canada) and stained intracellularly using PE-conjugated mouse anti-p24 mAb (clone KC57; Beckman Coulter, Brea, CA, USA; 1:100 dilution). The percentage of infected cells (p24+) was determined by gating the living cell population according to dye staining (Aqua Vivid; Thermo Fisher Scientific). Samples were acquired on an LSR II cytometer (BD Biosciences), and data analysis was performed using FlowJo v10.5.3 (Tree Star, Ashland, OR, USA).

Luciferase-based ADCC assay. The luciferase-based ADCC assay was performed according to a previously published protocol (37, 43). Briefly, CEM.NKr-CCR5 cells with LTR-Luc were infected by spinoculation in round-bottom tubes. The target cells (5×10^5) and infectious viral inoculum were subjected to centrifugation at 1,200 $\times$ *g* for 2 h at 25°C. Then, the viral inoculum was removed, and the target cells were cultured in R10 medium for 2 days. Target cells were washed three times in R10 medium and suspended in R10 medium containing 10 U/mL IL-2 without Cyclosporine (CsA). In flat-bottom, tissue culture-treated, polystyrene 96-well black plates, 40 μL each of the target and effector cells were added at 2.5×10^5 cells/mL and 2.5×10^6 cells/mL, respectively. YIR-821 was applied with the target cells at concentrations of 20 μM (Fig. 8). N6 effector cells and uninfected target cells were a control to define 0% RLU. N6 cells and infected targets without antibody were a control to define 100% RLU. Antibodies (20 μL) were added in sextuplicate. After 8 h of incubation, 100 μL of BriteLite Plus (Perkin Elmer) was added. Luciferase activity was measured using an EnSpire multimode plate reader, and the percentage of killing of HIV-1-infected cells was calculated from the decrease in RLUs.

FACS-based ADCC assay. The FACS-based ADCC assay was performed according to a previously published protocol (45). Briefly, infected primary $CD4^+$ T cells were stained with AquaVivid viability dye and a cell proliferation dye (eFluor670; eBioscience) and were used as target cells. Autologous effector PBMCs, stained with another cellular marker (cell proliferation dye eFluor450), were added at an effector/target ratio of 10:1 in 96-well V-bottom plates (Corning). The indicated concentrations of ADCC-mediating mAbs (5 μg/mL) or plasma (1:1,000) along with 50 μM BNM-III-170, YIR-821, or equivalent amounts of dimethyl sulfoxide (DMSO), when specified, were added to appropriate wells and cells were incubated for 15 min at RT. The plates were subsequently centrifuged for 1 min at 300 $\times$ *g* and then incubated at 37°C and 5% CO_2 for 5 h before being fixed in a 2% PBS-formaldehyde solution. Infected cells were identified by intracellular p24 staining, as described above. Samples were analyzed on an LSRII cytometer (BD Biosciences), and data analysis was performed using FlowJo v10.5.3X (Tree Star). The percentage of ADCC was calculated by gating infected live target cells according to the following formula: ([% of $p24^+$ cells in targets + effectors] − [% of $p24^+$ cells in targets + effectors + plasma]/[% of $p24^+$ cells in targets] $\times$ 100).

Protein purification and crystallization. Clade A/E 93TH057gp120 $core_e$ with LM (His^{61} to Tyr, Gln^{105} to His, Val^{108} to Ile, Asn^{474} to Asp, Ile^{475} to Met, and Lys^{476} to Arg) and HT (His^{375} to Thr) mutations (24) was prepared by transfection of GnT1-HEK 293F FreeStyle cells (Thermo Fisher Scientific) with 0.5 mg of plasmid/L of culture. Cells were grown in FreeStyle 293 medium (Thermo Fisher Scientific) supplemented with 0.5% Ultra Low IgG FBS (Gibco) in 8% CO_2 for 7 days. Cells were pelleted, the medium was filtered, and gp120 was purified from the medium by passage through a 17b affinity column made by covalently linking the anti-gp120 antibody 17b to protein A agarose. Then, gp120 was eluted from the column with 0.1 M glycine pH 3.0 and the pH was immediately raised after elution by the addition of 1 M Tris-HCl pH 8.5. The protein was concentrated, the buffer was exchanged for 50 mM sodium

acetate pH 6.0 and 300 mM sodium chloride, and the glycans were truncated by incubation at 37°C overnight in the presence of Endo H_f (New England Biolabs). Endo H_f was removed by passage through an amylose column and the gp120 was further purified by size exclusion chromatography through a Superdex 200 gel filtration column (GE Healthcare) equilibrated in 20 mM Tris-HCl pH 7.2 and 100 mM ammonium acetate prior to use in crystallization trials.

Deglycosylated LM/HT 93TH057 gp120 $core_e$ (5 mg/mL) was crystalized by the hanging drop method in 5 to 10% PEG 1500, 5% PEG 400, and 0.1 M HEPES pH 7.5. YIR-821 was solubilized with DMSO to a final concentration of 10 mM and diluted with crystallization buffer to 200 nM before addition to crystals. Briefly, 0.4 μL of 200 nM YIR-821 was added to the 0.4 μL hanging drop containing gp120 crystals. Crystals were allowed to incubate with the compound for 4 h and were then flash-frozen in liquid nitrogen after a brief soak in crystallization buffer containing 20% (+/−)-MPD for cryoprotection and 200 nM YIR-821.

Data collection, structure determination, and refinement. Data were collected on the Stanford Synchrotron Radiation Light Source (SSRL) beamline 12-2 on a Dectris Pilatus 6M detector. Data were integrated and processed with HKL3000 (46) and MOSFLM and SCALA from the CCP4 suite (47). Crystals were orthorhombic belonging to space group $P2_12_12_1$ with cell dimensions of a = 65.7 Å, b = 67.3 Å, and c = 87.4 Å, diffracted to 3.2 Å. Structures were solved by molecular replacement with the program PHASER from the CCP4 suite using PDB ID 6ONF as a starting model. Model building was conducted using the program COOT (48). Refinement was conducted using the program REFMAC from the CCP4 suite (47) and PHENIX (49).

Structure validation and analysis. The quality of the final refined models was monitored using the program MolProbity (50). Structural alignments were performed using the program LSQKAB from the CCP4 suite (47). The PISA webserver was used to determine contact surfaces and residues and all illustrations were prepared with the PyMol molecular graphic suite (DeLano Scientific, San Carlos, CA, USA). Complete data collection and refinement statistics can be found in Table S4.

Data Availability. The GenBank accession numbers for the sequences are MZ147102–MZ147194, AB059296, AB059316, and OP169349–OP139377.

SUPPLEMENTAL MATERIAL

Supplemental material is available online only.

SUPPLEMENTAL FILE 1, PDF file, 1 MB.

ACKNOWLEDGMENTS

We gratefully acknowledge David T. Evans for NKR24 and N6 cells. The following reagent was obtained through the NIH AIDS Reagent Program, Division of AIDS, NIAID, NIH from D. C. Montefiori, F. Gao, M. Li, B. H. Hahn, J. F. Salazar-Gonzalez, X. Wei, G. M. Shaw, D. L. Kothe, S. Abdool Karim, G. Ramjee, C. Williamson, Y. Li, C. A. Derdeyn, E. Hunter, L. Morris, K. Mlisana, J. Overbaugh, J. C. Kappes, D. X. Wu, and Tranzyme Inc.: Panel of HIV-1 Subtype B Env Clones (cat. no. 11227), Panel of HIV-1 Subtype C Env Clones (cat. no. 11326), and Panel of Global HIV-1 Env Clones; from J. Overbaugh: Panel of HIV-1 Env Clones–Subtype A, AC, B/C, G (cat. no. 11947); from D. Ellenberger, B. Li, M. Callahan, and S. Buterra: Panel of HIV-1 Subtype A/G Env Clones (cat. no. 11673); from John C. Kappes and Xiaoyun Wu: pSG3ΔEnv (cat. no. 11051) and TZM-bl cells (cat. no. 8129); and from John Mascola: VRC01 mAb Heavy and Light Chain Expression Vectors (cat. no. 12035 and 12036). We thank K. Fox and D. Phil from Edanz Group (https://en-author-services.edanzgroup.com/ac) for editing a draft of the manuscript.

This work was supported in part by JST SPRING (grant no. JPMJSP2127), Global Education and Research Center Aiming at the Control of AIDS, JSPS KAKENHI (grant no. 18H0285400), and a grant for Research Program on HIV/AIDS from the Japan Agency for Medical Research and Development (JP19fk0410025h0001, JP20fk0410025h0002, JP21fk0410025h0003, and JP22fk0410054h0001). This work was also supported in part by JSPS KAKENHI (19H03703, 21K19657, and 22H03119), JSPS Bilateral Open Partnership Joint Research Projects (JSJSBP120219933), and JSPS Core-to-Core Program (JPJSCCB20190009 and JPJSCCB20220010) (to T.U.). Work in the Finzi lab was partially supported by a Canadian Institutes of Health Research (CIHR) foundation grant (grant no. 352417) to A.F. Funds were provided by the National Institutes of Health to M.P. and A.F. (R01 AI129769). Support for this work was also provided by P01 GM56550/AI150471 to A.B.S. and A.F. This work was partially supported by 1UM1AI164562-01, cofunded by National Heart, Lung and Blood Institute, National Institute of Diabetes and Digestive and Kidney Diseases, National Institute of Neurological Disorders and Stroke, National Institute on Drug Abuse, and the National Institute of Allergy and Infectious Diseases to A.F. Additionally, A.F. is the recipient of

a Canada Research Chair on Retroviral Entry (no. RCHS0235 950-232424). J.P. is the recipient of a CIHR doctoral fellowship.

Use of the Stanford Synchrotron Radiation Lightsource, SLAC National Accelerator Laboratory, is supported by the U.S. Department of Energy, Office of Science, Office of Basic Energy Sciences under contract no. DE-AC02-76SF00515. The SSRL Structural Molecular Biology Program is supported by the DOE Office of Biological and Environmental Research, and by the National Institutes of Health, National Institute of General Medical Sciences.

The funders had no role in study design, data collection and analysis, decision to publish, or preparation of the manuscript and the contents of this publication are solely the responsibility of the authors. The views expressed in the manuscript are those of the authors and do not reflect the official policy or position of the Uniformed Services University, the U.S. Army, the Department of Defense, or the US Government.

K.M., T. Kuwata, A.F., and S.M. conceived and designed the study. K.M., W.D.T., S.T., M.P., S.D., J.P., and J.R. performed experiments. W.D.T. and M.P. solved the crystal structure of gp120 core-YIR-821 complex. H.N., G.P.J., and T.U. prepared clinical samples. T. Kobayakawa, K.T., and H.T. prepared the CD4mc YIR-821. A.B.S. prepared JP-III-48 and BNM-III-170. K.M., T. Kuwata, W.D.T., M.P., A.F., J.R., A.B.S., and S.M. prepared the manuscript. All authors read, edited, and approved the final manuscript.

REFERENCES

1. Haim H, Si Z, Madani N, Wang L, Courter JR, Princiotto A, Kassa A, DeGrace M, McGee-Estrada K, Mefford M, Gabuzda D, Smith AB, III, Sodroski J. 2009. Soluble CD4 and CD4-mimetic compounds inhibit HIV-1 infection by induction of a short-lived activated state. PLoS Pathog 5:e1000360. https://doi.org/10.1371/journal.ppat.1000360.
2. Madani N, Princiotto AM, Zhao C, Jahanbakhshsefidi F, Mertens M, Herschhorn A, Melillo B, Smith AB, III, Sodroski J. 2017. Activation and inactivation of primary human immunodeficiency virus envelope glycoprotein trimers by CD4-mimetic compounds. J Virol 91:e01880-16. https://doi.org/10.1128/JVI.01880-16.
3. Tolbert WD, Gohain N, Veillette M, Chapleau JP, Orlandi C, Visciano ML, Ebadi M, DeVico AL, Fouts TR, Finzi A, Lewis GK, Pazgier M. 2016. Paring down HIV env: design and crystal structure of a stabilized inner domain of HIV-1 gp120 displaying a major ADCC target of the A32 region. Structure 24:697–709. https://doi.org/10.1016/j.str.2016.03.005.
4. Alsahafi N, Bakouche N, Kazemi M, Richard J, Ding S, Bhattacharyya S, Das D, Anand SP, Prévost J, Tolbert WD, Lu H, Medjahed H, Gendron-Lepage G, Ortega Delgado GG, Kirk S, Melillo B, Mothes W, Sodroski J, Smith AB, III, Kaufmann DE, Wu X, Pazgier M, Rouiller I, Finzi A, Munro JB. 2019. An asymmetric opening of HIV-1 envelope mediates antibody-dependent cellular cytotoxicity. Cell Host Microbe 25:578–587.e5. https://doi.org/10.1016/j.chom.2019.03.002.
5. Richard J, Prévost J, Alsahafi N, Ding S, Finzi A. 2018. Impact of HIV-1 envelope conformation on ADCC responses. Trends Microbiol 26:253–265. https://doi.org/10.1016/j.tim.2017.10.007.
6. Munro JB, Gorman J, Ma X, Zhou Z, Arthos J, Burton DR, Koff WC, Courter JR, Smith AB, III, Kwong PD, Blanchard SC, Mothes W. 2014. Conformational dynamics of single HIV-1 envelope trimers on the surface of native virions. Science 346:759–763. https://doi.org/10.1126/science.1254426.
7. Richard J, Veillette M, Brassard N, Iyer SS, Roger M, Martin L, Pazgier M, Schön A, Freire E, Routy JP, Smith AB, III, Park J, Jones DM, Courter JR, Melillo BN, Kaufmann DE, Hahn BH, Permar SR, Haynes BF, Madani N, Sodroski JG, Finzi A. 2015. CD4 mimetics sensitize HIV-1-infected cells to ADCC. Proc Natl Acad Sci U S A 112:E2687–E2694. https://doi.org/10.1073/pnas.1506755112.
8. Richard J, Pacheco B, Gohain N, Veillette M, Ding S, Alsahafi N, Tolbert WD, Prévost J, Chapleau JP, Coutu M, Jia M, Brassard N, Park J, Courter JR, Melillo B, Martin L, Tremblay C, Hahn BH, Kaufmann DE, Wu X, Smith AB, III, Sodroski J, Pazgier M, Finzi A. 2016. Co-receptor binding site antibodies enable CD4-mimetics to expose conserved anti-cluster A ADCC epitopes on HIV-1 envelope glycoproteins. EBioMedicine 12:208–218. https://doi.org/10.1016/j.ebiom.2016.09.004.
9. Rajashekar JK, Richard J, Beloor J, Prévost J, Anand SP, Beaudoin-Bussières G, Shan L, Herndler-Brandstetter D, Gendron-Lepage G, Medjahed H, Bourassa C, Gaudette F, Ullah I, Symmes K, Peric A, Lindemuth E, Bibollet-Ruche F, Park J, Chen HC, Kaufmann DE, Hahn BH, Sodroski J, Pazgier M, Flavell RA, Smith AB, III, Finzi A, Kumar P. 2021. Modulating HIV-1 envelope glycoprotein conformation to decrease the HIV-1 reservoir. Cell Host Microbe 29:904–916.e6. https://doi.org/10.1016/j.chom.2021.04.014.
10. Yamada Y, Ochiai C, Yoshimura K, Tanaka T, Ohashi N, Narumi T, Nomura W, Harada S, Matsushita S, Tamamura H. 2010. CD4 mimics targeting the mechanism of HIV entry. Bioorg Med Chem Lett 20:354–358. https://doi.org/10.1016/j.bmcl.2009.10.098.
11. Narumi T, Arai H, Yoshimura K, Harada S, Nomura W, Matsushita S, Tamamura H. 2011. Small molecular CD4 mimics as HIV entry inhibitors. Bioorg Med Chem 19:6735–6742. https://doi.org/10.1016/j.bmc.2011.09.045.
12. Hashimoto C, Narumi T, Otsuki H, Hirota Y, Arai H, Yoshimura K, Harada S, Ohashi N, Nomura W, Miura T, Igarashi T, Matsushita S, Tamamura H. 2013. A CD4 mimic as an HIV entry inhibitor: pharmacokinetics. Bioorg Med Chem 21:7884–7889. https://doi.org/10.1016/j.bmc.2013.10.005.
13. Narumi T, Arai H, Yoshimura K, Harada S, Hirota Y, Ohashi N, Hashimoto C, Nomura W, Matsushita S, Tamamura H. 2013. CD4 mimics as HIV entry inhibitors: lead optimization studies of the aromatic substituents. Bioorg Med Chem 21:2518–2526. https://doi.org/10.1016/j.bmc.2013.02.041.
14. Otsuki H, Hishiki T, Miura T, Hashimoto C, Narumi T, Tamamura H, Yoshimura K, Matsushita S, Igarashi T. 2013. Generation of a replication-competent simian-human immunodeficiency virus, the neutralization sensitivity of which can be enhanced in the presence of a small-molecule CD4 mimic. J Gen Virol 94:2710–2716. https://doi.org/10.1099/vir.0.055590-0.
15. Mizuguchi T, Harada S, Miura T, Ohashi N, Narumi T, Mori H, Irahara Y, Yamada Y, Nomura W, Matsushita S, Yoshimura K, Tamamura H. 2016. A minimally cytotoxic CD4 mimic as an HIV entry inhibitor. Bioorg Med Chem Lett 26:397–400. https://doi.org/10.1016/j.bmcl.2015.11.103.
16. Ohashi N, Harada S, Mizuguchi T, Irahara Y, Yamada Y, Kotani M, Nomura W, Matsushita S, Yoshimura K, Tamamura H. 2016. Small-Molecule CD4 Mimics Containing Mono-cyclohexyl Moieties as HIV Entry Inhibitors. ChemMedChem 11:940–946. https://doi.org/10.1002/cmdc.201500590.
17. Kobayakawa T, Tsuji K, Konno K, Himeno A, Masuda A, Yang T, Takahashi K, Ishida Y, Ohashi N, Kuwata T, Matsumoto K, Yoshimura K, Sakawaki H, Miura T, Harada S, Matsushita S, Tamamura H. 2021. Hybrids of small-molecule CD4 mimics with polyethylene glycol units as HIV entry inhibitors. J Med Chem 64:1481–1496. https://doi.org/10.1021/acs.jmedchem.0c01153.
18. Ramirez Valdez KP, Kuwata T, Maruta Y, Tanaka K, Alam M, Yoshimura K, Matsushita S. 2015. Complementary and synergistic activities of anti-V3, CD4bs and CD4i antibodies derived from a single individual can cover a wide range of HIV-1 strains. Virology 475:187–203. https://doi.org/10.1016/j.virol.2014.11.011.
19. Tanaka K, Kuwata T, Alam M, Kaplan G, Takahama S, Valdez KPR, Roitburd-Berman A, Gershoni JM, Matsushita S. 2017. Unique binding modes for the broad neutralizing activity of single-chain variable fragments (scFv) targeting CD4-induced epitopes. Retrovirology 14:44. https://doi.org/10.1186/s12977-017-0369-y.
20. Thida W, Kuwata T, Maeda Y, Yamashiro T, Tran GV, Nguyen KV, Takiguchi M, Gatanaga H, Tanaka K, Matsushita S. 2019. The role of conventional

antibodies targeting the CD4 binding site and CD4-induced epitopes in the control of HIV-1 CRF01_AE viruses. Biochem Biophys Res Commun 508:46–51. https://doi.org/10.1016/j.bbrc.2018.11.063.
21. Wang FX, Kimura T, Nishihara K, Yoshimura K, Koito A, Matsushita S. 2002. Emergence of autologous neutralization-resistant variants from preexisting human immunodeficiency virus (HIV) quasi species during virus rebound in HIV type 1-infected patients undergoing highly active antiretroviral therapy. J Infect Dis 185:608–617. https://doi.org/10.1086/339015.
22. Morikita T, Maeda Y, Fujii S, Matsushita S, Obaru K, Takatsuki K. 1997. The V1/V2 region of human immunodeficiency virus type 1 modulates the sensitivity to neutralization by soluble CD4 and cellular tropism. AIDS Res Hum Retroviruses 13:1291–1299. https://doi.org/10.1089/aid.1997.13.1291.
23. Judicate GP, Barabona G, Kamori D, Mahiti M, Tan TS, Ozono S, Mgunya AS, Kuwata T, Matsushita S, Sunguya B, Lyamuya E, Tokunaga K, Ueno T. 2021. Phenotypic and Genotypic Co-receptor Tropism Testing in HIV-1 epidemic region of Tanzania where multiple non-b subtypes co-circulate. Front Microbiol 12:703041. https://doi.org/10.3389/fmicb.2021.703041.
24. Prévost J, Tolbert WD, Medjahed H, Sherburn RT, Madani N, Zoubchenok D, Gendron-Lepage G, Gaffney AE, Grenier MC, Kirk S, Vergara N, Han C, Mann BT, Chénine AL, Ahmed A, Chaiken I, Kirchhoff F, Hahn BH, Haim H, Abrams CF, Smith AB, III, Sodroski J, Pazgier M, Finzi A. 2020. The HIV-1 Env gp120 inner domain shapes the Phe43 Cavity and the CD4 binding site. mBio 11:e00280-20. https://doi.org/10.1128/mBio.00280-20.
25. Zhao Q, Ma L, Jiang S, Lu H, Liu S, He Y, Strick N, Neamati N, Debnath AK. 2005. Identification of N-phenyl-N'-(2,2,6,6-tetramethyl-piperidin-4-yl)-oxalamides as a new class of HIV-1 entry inhibitors that prevent gp120 binding to CD4. Virology 339:213–225. https://doi.org/10.1016/j.virol.2005.06.008.
26. Melillo B, Liang S, Park J, Schon A, Courter JR, LaLonde JM, Wendler DJ, Princiotto AM, Seaman MS, Freire E, Sodroski J, Madani N, Hendrickson WA, Smith AB, III. 2016. Small-molecule cd4-mimics: structure-based optimization of HIV-1 entry inhibition. ACS Med Chem Lett 7:330–334. https://doi.org/10.1021/acsmedchemlett.5b00471.
27. Laumaea A, Smith AB, III, Sodroski J, Finzi A. 2020. Opening the HIV envelope: potential of CD4 mimics as multifunctional HIV entry inhibitors. Curr Opin HIV AIDS 15:300–308. https://doi.org/10.1097/COH.0000000000000637.
28. Selhorst P, Grupping K, Tong T, Crooks ET, Martin L, Vanham G, Binley JM, Ariën KK. 2013. M48U1 CD4 mimetic has a sustained inhibitory effect on cell-associated HIV-1 by attenuating virion infectivity through gp120 shedding. Retrovirology 10:12. https://doi.org/10.1186/1742-4690-10-12.
29. Anang S, Richard J, Bourassa C, Goyette G, Chiu TJ, Chen HC, Smith AB, III, Madani N, Finzi A, Sodroski J. 2022. Characterization of human immunodeficiency virus (HIV-1) envelope glycoprotein variants selected for resistance to a CD4-mimetic compound. J Virol 96:e0063622. https://doi.org/10.1128/jvi.00636-22.
30. Daar ES, Li XL, Moudgil T, Ho DD. 1990. High concentrations of recombinant soluble CD4 are required to neutralize primary human immunodeficiency virus type 1 isolates. Proc Natl Acad Sci U S A 87:6574–6578. https://doi.org/10.1073/pnas.87.17.6574.
31. Pacheco B, Alsahafi N, Debbeche O, Prévost J, Ding S, Chapleau JP, Herschhorn A, Madani N, Princiotto A, Melillo B, Gu C, Zeng X, Mao Y, Smith AB, III, Sodroski J, Finzi A. 2017. Residues in the gp41 ectodomain regulate HIV-1 envelope glycoprotein conformational transitions induced by gp120-directed inhibitors. J Virol 91:e02219-16. https://doi.org/10.1128/JVI.02219-16.
32. Fontaine J, Chagnon-Choquet J, Valcke HS, Poudrier J, Roger M, Montreal Primary HIV Infection and Long-Term Non-Progressor Study Groups. 2011. High expression levels of B lymphocyte stimulator (BLyS) by dendritic cells correlate with HIV-related B-cell disease progression in humans. Blood 117:145–155. https://doi.org/10.1182/blood-2010-08-301887.
33. Fontaine J, Coutlée F, Tremblay C, Routy JP, Poudrier J, Roger M, Montreal Primary HIV Infection and Long-Term Nonprogressor Study Groups. 2009. HIV infection affects blood myeloid dendritic cells after successful therapy and despite nonprogressing clinical disease. J Infect Dis 199:1007–1018. https://doi.org/10.1086/597278.
34. Pereyra F, Jia X, McLaren PJ, Telenti A, de Bakker PI, Walker BD, Ripke S, Brumme CJ, Pulit SL, Carrington M, Kadie CM, Carlson JM, Heckerman D, Graham RR, Plenge RM, Deeks SG, Gianniny L, Crawford G, Sullivan J, Gonzalez E, Davies L, Camargo A, Moore JM, Beattie N, Gupta S, Crenshaw A, Burtt NP, Guiducci C, Gupta N, Gao X, Qi Y, Yuki Y, Piechocka-Trocha A, Cutrell E, Rosenberg R, Moss KL, Lemay P, O'Leary J, Schaefer T, Verma P, Toth I, Block B, Baker B, Rothchild A, Lian J, Proudfoot J, Alvino DM, Vine S, Addo MM, Allen TM, International HIV Controllers Study, et al. 2010. The major genetic determinants of HIV-1 control affect HLA class I peptide presentation. Science 330:1551–1557. https://doi.org/10.1126/science.1195271.
35. Kamya P, Boulet S, Tsoukas CM, Routy JP, Thomas R, Côté P, Boulassel MR, Baril JG, Kovacs C, Migueles SA, Connors M, Suscovich TJ, Brander C, Tremblay CL, Bernard N, Canadian Cohort of HIV Infected Slow Progressors. 2011. Receptor-ligand requirements for increased NK cell polyfunctional potential in slow progressors infected with HIV-1 coexpressing KIR3DL1*h/*y and HLA-B*57. J Virol 85:5949–5960. https://doi.org/10.1128/JVI.02652-10.
36. Peretz Y, Ndongala ML, Boulet S, Boulassel MR, Rouleau D, Côté P, Longpré D, Routy JP, Falutz J, Tremblay C, Tsoukas CM, Sékaly RP, Bernard NF. 2007. Functional T cell subsets contribute differentially to HIV peptide-specific responses within infected individuals: correlation of these functional T cell subsets with markers of disease progression. Clin Immunol 124:57–68. https://doi.org/10.1016/j.clim.2007.04.004.
37. Alpert MD, Heyer LN, Williams DE, Harvey JD, Greenough T, Allhorn M, Evans DT. 2012. A novel assay for antibody-dependent cell-mediated cytotoxicity against HIV-1- or SIV-infected cells reveals incomplete overlap with antibodies measured by neutralization and binding assays. J Virol 86:12039–12052. https://doi.org/10.1128/JVI.01650-12.
38. Tsuji K, Kobayakawa T, Konno K, Masuda A, Takahashi K, Ohashi N, Yoshimura K, Kuwata T, Matsushita S, Harada S, Tamamura H. 2022. Exploratory studies on soluble small molecule CD4 mimics as HIV entry inhibitors. Bioorg Med Chem 56:116616. https://doi.org/10.1016/j.bmc.2022.116616.
39. Thali M, Moore JP, Furman C, Charles M, Ho DD, Robinson J, Sodroski J. 1993. Characterization of conserved human immunodeficiency virus type 1 gp120 neutralization epitopes exposed upon gp120-CD4 binding. J Virol 67:3978–3988. https://doi.org/10.1128/JVI.67.7.3978-3988.1993.
40. Guan Y, Pazgier M, Sajadi MM, Kamin-Lewis R, Al-Darmarki S, Flinko R, Lovo E, Wu X, Robinson JE, Seaman MS, Fouts TR, Gallo RC, DeVico AL, Lewis GK. 2013. Diverse specificity and effector function among human antibodies to HIV-1 envelope glycoprotein epitopes exposed by CD4 binding. Proc Natl Acad Sci U S A 110:E69–E78. https://doi.org/10.1073/pnas.1217609110.
41. Kuwata T, Enomoto I, Baba M, Matsushita S. 2016. Incompatible natures of the HIV-1 envelope in resistance to the CCR5 antagonist cenicriviroc and to neutralizing antibodies. Antimicrob Agents Chemother 60:437–450. https://doi.org/10.1128/AAC.02285-15.
42. Montefiori DC. 2009. Measuring HIV neutralization in a luciferase reporter gene assay. Methods Mol Biol 485:395–405. https://doi.org/10.1007/978-1-59745-170-3_26.
43. Md Zahid H, Kuwata T, Takahama S, Kaku Y, Biswas S, Matsumoto K, Tamamura H, Matsushita S. 2021. Functional analysis of a monoclonal antibody reactive against the C1C2 of Env obtained from a patient infected with HIV-1 CRF02_AG. Retrovirology 18:23. https://doi.org/10.1186/s12977-021-00568-y.
44. Edmonds TG, Ding H, Yuan X, Wei Q, Smith KS, Conway JA, Wieczorek L, Brown B, Polonis V, West JT, Montefiori DC, Kappes JC, Ochsenbauer C. 2010. Replication competent molecular clones of HIV-1 expressing Renilla luciferase facilitate the analysis of antibody inhibition in PBMC. Virology 408:1–13. https://doi.org/10.1016/j.virol.2010.08.028.
45. Anand SP, Prévost J, Baril S, Richard J, Medjahed H, Chapleau JP, Tolbert WD, Kirk S, Smith AB, III, Wines BD, Kent SJ, Hogarth PM, Parsons MS, Pazgier M, Finzi A. 2019. Two families of env antibodies efficiently engage fc-gamma receptors and eliminate HIV-1-infected cells. J Virol 93:e01823-18. https://doi.org/10.1128/JVI.01823-18.
46. Otwinowski Z, Minor W. 1997. Processing of X-ray diffraction data collected in oscillation mode. Methods Enzymol 276:307–326. https://doi.org/10.1016/S0076-6879(97)76066-X.
47. Collaborative Computational Project N. 1994. The CCP4 suite: programs for protein crystallography. Acta Crystallogr D Biol Crystallogr 50:760–763. https://doi.org/10.1107/S0907444994003112.
48. Emsley P, Cowtan K. 2004. Coot: model-building tools for molecular graphics. Acta Crystallogr D Biol Crystallogr 60:2126–2132. https://doi.org/10.1107/S0907444904019158.
49. Adams PD, Afonine PV, Bunkoczi G, Chen VB, Davis IW, Echols N, Headd JJ, Hung LW, Kapral GJ, Grosse-Kunstleve RW, McCoy AJ, Moriarty NW, Oeffner R, Read RJ, Richardson DC, Richardson JS, Terwilliger TC, Zwart PH. 2010. PHENIX: a comprehensive Python-based system for macromolecular structure solution. Acta Crystallogr D Biol Crystallogr 66:213–221. https://doi.org/10.1107/S0907444909052925.
50. Davis IW, Murray LW, Richardson JS, Richardson DC. 2004. MOLPROBITY: structure validation and all-atom contact analysis for nucleic acids and their complexes. Nucleic Acids Res 32:W615–W619. https://doi.org/10.1093/nar/gkh398.